Bull. Disas. Prev. Res. Inst., Kyoto Univ., Vol.20, Part 3, No.177, March 1971

On the Nature of the Occurrence of Intermediate and Deep Earthquakes. 1. The World Wide Distribution of the Earthquake Generating Stress.

By Kazuo OIKE

(Manuscript received December 28, 1970)

Abstract

The world wide distribution of the earthquake generating stress of intermediate and deep earthquakes has been mainly obtained from the smoothed radiation patterns of P Waves of groups of earthquakes in fifty-one seimically active regions. And these results were compared with the fault plane solutions of individual earthquakes in the same regions.

Data used in this study were taken from the Bulletins of the International Seismological Center, 1964 and 1965 for the very active regions; and for the regions where a few intermediate and deep earthquakes occurred data from the Earthquake Data Reports of the U. S. Coast and Geodetic Survey, 1966-1969, were added.

The smoothed radiation patterns of the Kuril-Japan, the Izu-Marianas and the Tonga-Kermadec regions determined from only two years' data showed satisfactory agreement with the patterns obtained for larger earthquakes by many seismologists.

In almost all regions the axes ofmaximum pressure align themselves with the dip of the seismic plane. The direction of the horizontal component of the axis of maximum pressure in each region was compared with the direction of differential movement between two blocks computed by Le Pichon, and they agreed well with each other except in the following regions. In the South America region, the axes of maximum pressure lie in the NW-SE direction, while the vectors of the differential movement lie in the east-west direction. The patterns of intermediate earthquakes of the Chile-Peru border region, the Honshu of Japan and the New Hebrides region show that the axes of maximum tension align themselves with the dip of the seimic plane.

1. Introduction

One of the significant data which supported the new global tectonics developed by Isacks et al. (1968) was the earthquake generating stress determined from the fault plane solutions of comparatively large earthquakes.[1] The fault plane solutions of intermediate and deep earthquakes in and near Japan were determined by Honda et al. (1967),[2] Ichikawa (1966),[3] and Katsumata and Sykes (1969).[4] The solutions for the Tonga-Kermadec region were obtained by Isacks et al. (1969).[5] These solutions were interpreted by a tectonic model which was termed the new global tectonics.

Although numerous descriptions of the focal mechanism have been presented by many seismologists and have contributed to the developement of tectonophysics, there are some regions where the earthquake generating stress especially of intermediate and deep earthquakes have not yet been determined in detail, because in these regions there are neither large earthquakes nor appropriate distribution of observation stations.

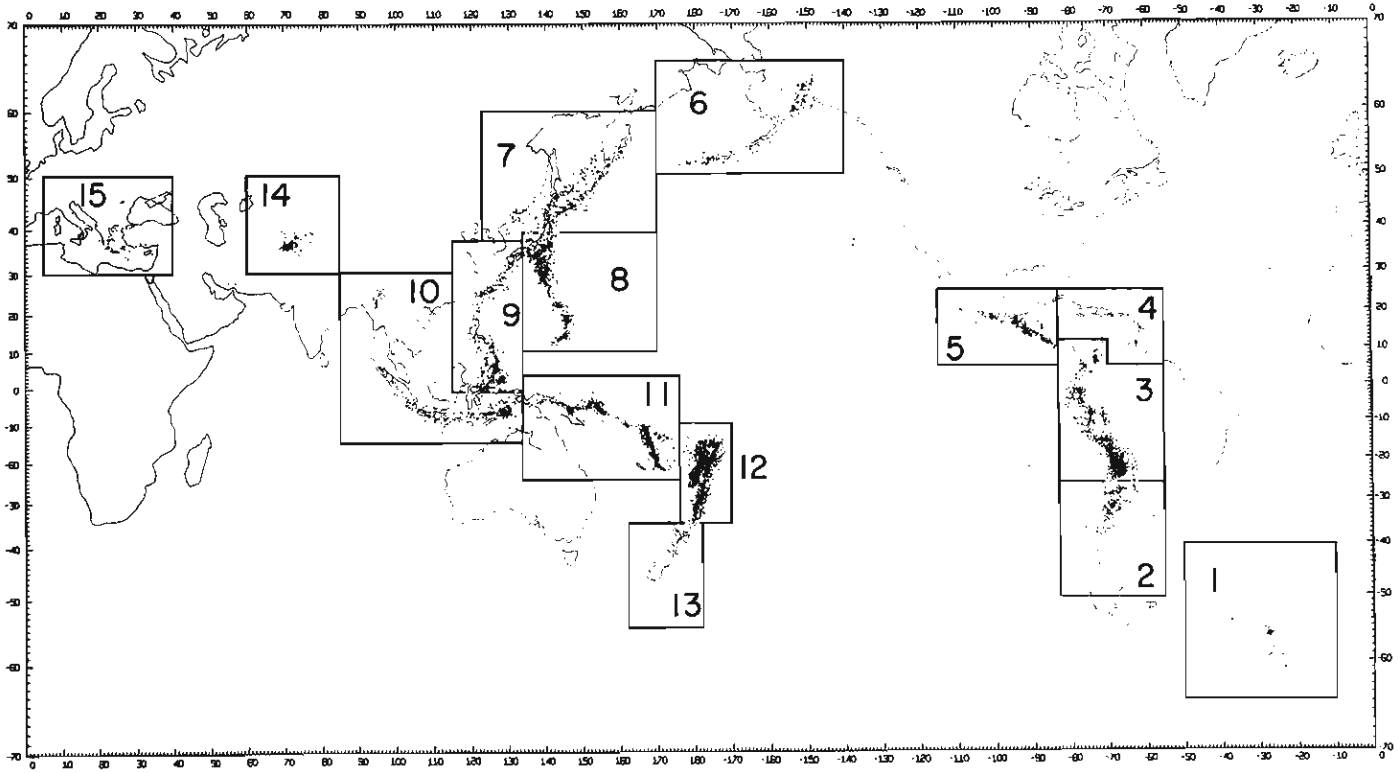

Fig. 1. Fifteen active regions of intermediate and deep earthquakes. The seismicity map refers to Barazangi and Dorman (1969).

The island arc or the continental margin where intermediate and deep earthquakes occur is the principal zone of tectonic activity. Therefore it is important to determine the earthquake generating stress of the intermediate and deep earthquakes in all these regions.

In this study the axes of maximum pressure and maximum tension of the generating stress of the intermediate and deep earthquakes in each region have been mainly determined from the smoothed radiation patterns of the initial P motions, superposing on them the distribution of first motions of a group of earthquakes in the region. This method is efficient and appropriate for the study of the principal axes of stress in restricted region, because the axes of intermediate and deep earthquakes are distributed systematically along the seismic belt, for example in and near Japan.

It is also useful in a detailed study of the earthquake generating stress of the small shocks when there is not sufficient data to determine the individual fault plane solutions. [6]

It seems that the systematic distribution in space of the principal axes of stress determined from the fault plane solutions of intermediate and deep earthquakes indicates their correspondence with the principal axes of the stress field in the region, as was mentioned by McKenzie (1969). [7] Then the average orientation of the principal axes obtained from the smoothed radiation patterns is regarded as the result directly related to the general feature of the tectonic force in the region concerned.

2. Data

Intermediate and deep earthquakes with focal depth of more than 100 km which occurred in the whole world from the beginning of 1964 to the end of 1969 have been analysed. The data of hypocenters, magnitude and the directions of initial P motions observed at the stations whose epicentral distances are less than 100 degrees are adopted from the Bulletins of the International Seismological Center for the first two years and from the Earthquake Data Reports of the U. S. Coast and Geodetic Survey for the last four years.

With reference to the world seismicity map compiled from ESSA, Coast and Geodetic Survey, epicenter data of 100–700 km deep, 1961–1967, by Barazangi and Dorman (1969), [8] the seismic active zones were classified into fifteen regions shown in Fig. 1. Initial P data in each region were adopted according to certain conditions shown in Table 1. The total number of earthquakes and the initial P data used for analysis are shown in Table 1.

The relation between the magnitude and the number of reported P data of each earthquake for three regions for the first two years is shown in Fig. 2. In the Izu-Mariana Islands region (8), the farther away the epicenter is from the network of the Japan Meteorological Agency, the fewer initial P data are reported. More than five P data are generally reported for any earthquake with a magnitude larger than 4.5 in each region. To obtain the fault plane solution of an individual earthquake, it is necessary that sufficient data with adequate distribution of azimuth and incident angle be reported. The relation in Fig. 2 shows that such earthquakes must have a magnitude larger than about 5.0.

Table 1. Conditions for the data sampling in each region; the period and the lower limits of magnitude and number of reported P data of each earthquake, and the data adopted; N_P: the number of the reported initial P data, N_e: the total number of earthquakes, N_c: the total number of compressions and N_d: the total number of dilatations.

No.	Region	Period	$M \geq$	$N_P \geq$	N_e	ΣN_P	ΣN_d	ΣN_c
1	South Sandwich Is.	1964—1965	3.0	1	32	234	85	149
		1966—1969	4.5	3				
2	Chile	1964—1965	3.0	1	61	330	141	189
		1966—1969	4.0	3				
3	Colombia-Peru-Bolivia	1964—1965	4.0	5	183	2,907	1,793	1,114
		1966—1969	4.5	10				
4	Dominica-Trinidad Tobago	1964—1965	3.0	1	38	247	91	156
		1966—1969	4.0	3				
5	Central America	1964—1965	3.0	1	77	678	117	561
		1966—1969	4.5	10				
6	Alaska-Aleutian	1964—1965	3.0	1	42	284	119	165
		1966—1969	3.0	10				
7	Kuril-Japan	1964—1965	4.0	5	65	2,084	1,061	1,023
8	Japan-Izu-Marianas	1964—1965	4.0	5	69	2,240	1,301	939
9	Ryukyu-Philippines	1964—1965	4.0	5	99	1,825	839	986
		1966—1969	4.5	10				
10	Indonesia	1964—1965	4.0	5	74	1,390	581	809
11	Solomon-New Hebrides	1964—1965	4.0	5	104	1,457	682	775
12	Fiji-Tonga-Kermadec	1964—1965	4.0	10	116	2,254	1,344	910
13	New Zealand	1964—1965	4.0	3	44	247	106	141
14	Afghanistan	1964—1965	4.0	5	53	1,055	470	585
15	Italy-Greece-Turkey	1964—1965	3.0	1	16	243	99	144

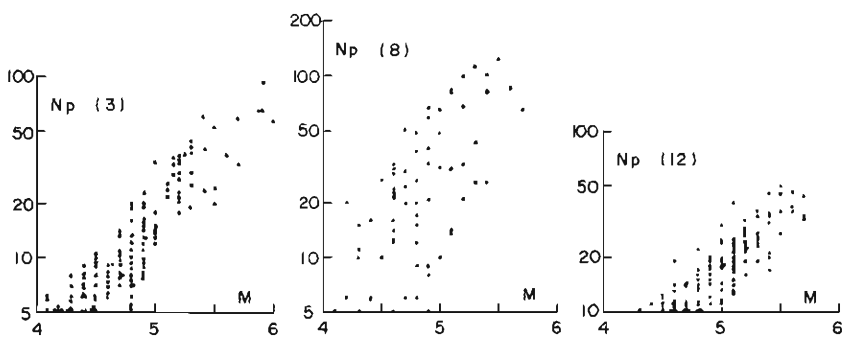

Fig. 2. Relation between the magnitude and the number of reported initial P data of each earthquake for the Colombia-Peru-Bolivia region (3), the Japan- Izu-Mariana region (8) and the Tonga-Kermadec region (12).

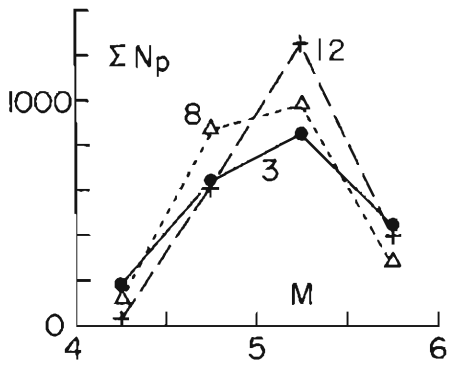

Fig. 3. Relation between the magnitude and the total number of the reported initial P data for the same regions in Fig. 2.

For the same three regions, the relation between the magnitude M and the total number of P data of earthquakes with the magnitude of $M \sim M+\Delta M$, ΣN_P, is shown in Fig. 3. It indicates that the smoothed radiation pattern composed from the summed-up distribution of P data well shows the nature of the generating stress of shocks with magnitude around 5.0. Then, the results can be compared with those of the larger earthquakes in the region where many fault plane solutions of individual earthquakes have been obtained.

The total number of earthquakes and of P data for them satisfying the conditions shown in Table 1, and the compressions and dilatations for each focal depth every 100 km are shown in Table 2 and Fig. 4. The relation between the total number of the compressions and the dilatations in each depth shown in Fig. 4 indicated that they are observed to be equal in number for intermediate earthquakes, but that for deep earthquakes the number of the dilatations is significantly larger than that of the compressions. This relationship in only those regions where deep earthquakes occur is similar to the same relation in the whole world. Hence, it is not a misleading pattern resulting from a biased distribution of observation stations. Such problems have been investigated by Randall and Knopoff (1970).[9),10)]

But it is not always necessary to consider the type of the focal mechanism of an individual earthquake to determine the principal axes of stress from the smoothed radiation pattern by Aki's method. In this paper the focal mechanism of intermediate and deep earthquakes is assumed to be the double-couple type which is equivalent to the slip dislocation model.

Table 2. Relation between the focal depth and the total number of P data (ΣN_P), the compressions (ΣN_c), and the dilatations (ΣN_d) of earthquakes of each depth for the whole world.

Depth (Km)	N_e	ΣN_P	ΣN_d	ΣN_c
100—200	693	9,589	4,473	5,116
200—300	154	2,299	1,153	1,146
300—400	45	1,174	547	627
400—500	57	1,580	905	675
500—600	85	1,946	1,124	822
600—700	39	887	627	260
Total	1,073	17,475	8,829	8,646

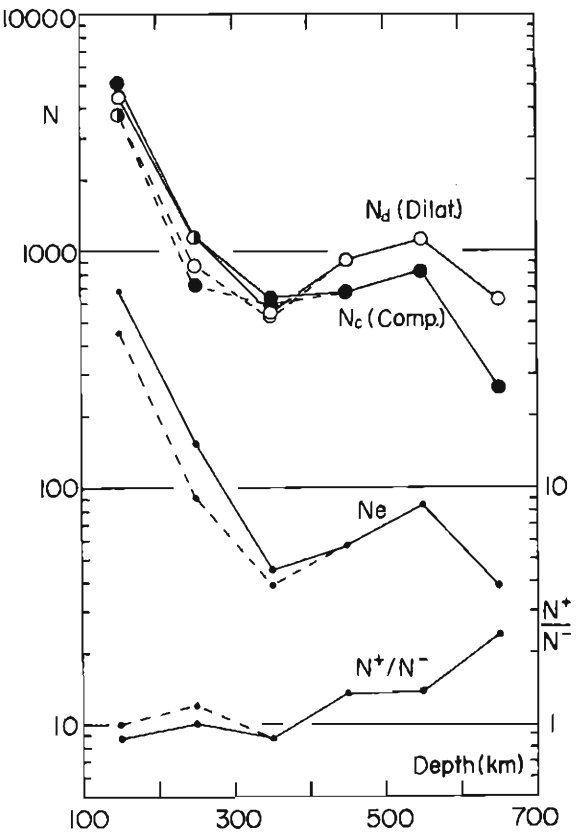

Fig. 4. Relation between the depth and the total number of dilatations and compressions, their ratio and the total number of earthquakes at each depth. Dotted lines indicate the results only in the regions where deep earthquakes occur (2, 3 and 7~12).

3. Methods to Determine the Earthquake Generating Stress

Two methods are used to find the average orientation of the principal axes of stress in each region. One is to determine the axes of maximum pressure and tension from the fault plane solutions of the larger individual earthquakes in the region. The results are shown in Table 4 and Fig. 37.

The other method is to determine a single solution for a group of earthquakes containing the smaller ones in the region, superposing the distribution of the first P motions regarded as if they were coming from a single source. This method was used by Aki (1966) to find the earthquake generating stress in Japan for the years 1961 to 1963.[10]

The distribution of signs of first motions superposed on a focal hemisphere is smoothed and normalized by the following procedure. The numer N_c of compressions and the number N_d of dilatations within an angular distance of 45° from

a point $Q(\theta, \varphi)$ and its antipode $Q'(\pi-\theta, \pi+\varphi)$ on a focal sphere are counted. Then, a normalized parameter $k(\theta, \varphi)$ is calculated by the following formula,

$$k=\frac{N_d-N_c}{N_d+N_c}.$$

The parameter k is calculated for 61 points of Q covering the surface of the lower hemi-sphere. $Q(\theta, \varphi)$ are distributed as follows:

($\theta=0°$, $\varphi=0°$),
($\theta=20°$, $\varphi=0°, 90°, 180°, 270°$),
($\theta=40°$, $\varphi=0°, 45°, 90°, 135°, 180°, 225°, 270°, 315°$),
($\theta=60°$, $\varphi=0°, 30°, 60°, 90°, 120°, 150°, 180°, 210°, 240°, 270°, 300°, 330°$),
($\theta=80°$, $\varphi=0°, 20°, 40°, 60°, 80°, 100°, 120°, 140°, 160°, 180°, 200°, 220°, 240°, 260°, 280°, 300°, 320°, 340°$), and
($\theta=90°$, $\varphi=0°, 20°, 40°, 60°, 80°, 100°, 120°, 140°, 160°, 180°, 200°, 220°, 240°, 260°, 280°, 300°, 320°, 340°$).

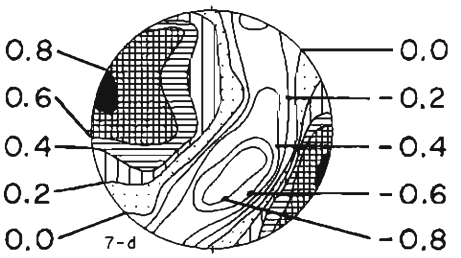

Fig. 5. An example of the smoothed radiation pattern indicated by the equal lines of k value. The maximum value of k corresponds to the axis of maximum pressure and the minimum corresponds to the axis of maximum tension.

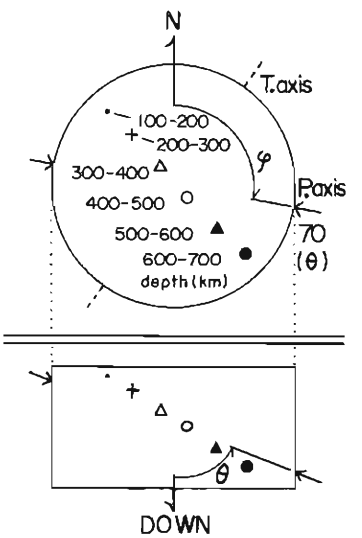

Fig. 6. Explanation of the expression of the data and the results in maps.

The values of k are plotted on the plane projected by Wulf's net and the equal lines of k are drawn as shown in Fig. 5. The maximum value of k on a focal sphere corresponds to the axis of maximum pressure and the minimum value corresponds to the axis of maximum tension.

The lines of equal k value of a group of earthquakes whose epicenters are within a circle of a certain radius and whose hypocenters are within the confines of the depth are shown in figures for each region. When the results for some areas showed the same pattern, they were compiled into a pattern for a broad region. The center and the radius of a circle, the boundaries of the depth, the number of sampled data and the results are listed in Table 3, The rank (A, B and C) in Table 3 indicates the reliability of the smoothed radiation

pattern depending on the distribution of the numbers of initial P data on a focal sphere.

The epicenters of earthquakes sampled by the conditions shown in Table 1 and the azimuths of the principal axes of stress obtained from the smoothed radiation pattern are shown on maps by the expression in Fig. 6.

4. Results Obtained for Each Region

a). *South Sandwich Islands.*

The smoothed radiation pattern and the distribution of the epicenters in this

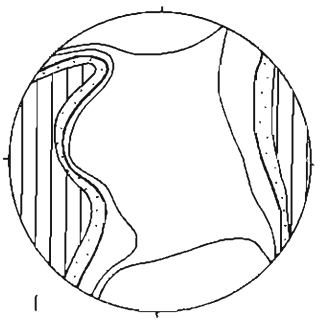

Fig. 7. Smoothed radiation pattern of the South Sandwich Island region.

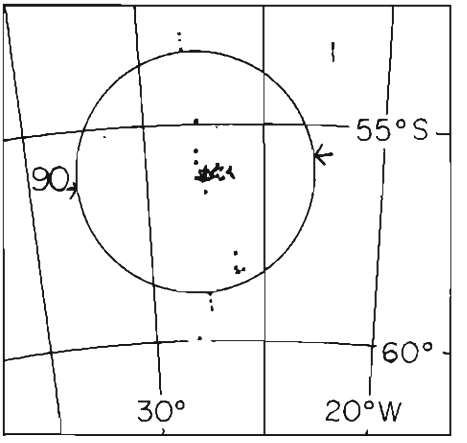

Fig. 8. Epicenter distribution and results for the South Sandwich Islands region.

region for the years 1964 to 1969 are shown in Figs. 7 and 8. They indicate that the axis of maximum pressure lies nearly horizontally in the direction perpendicular to the trend of the island arc and the trench. Two fault plane solutions in this region (No. 462 and 2492) are similar to this result.

But for earthquakes in this region, data from the near stations are not available. And so it is necessary to determine in detail the axes of the earthquake generating stress using not only P data but also data of other phases.

b). *South America.*

The patterns of intermediate earthquakes in Chile and deep earthquakes in Argentina for the years 1964 to 1969 are shown in the upper half of Fig. 9, and the lower half shows the patterns in the same regions for the first two years. No clear variation is found between these patterns of the different terms. These patterns show the horizontal axis of the maximum tension and the dipping axis of the maximum pressure in the south-east direction.

The results for the northern part of South America are shown in Fig. 10. Almost all patterns show that the axis of the maximum tension lies nearly horizontally in the NE-SW direction and the axis of the maximum pressure dips rather vertically in the NW-SE direction.

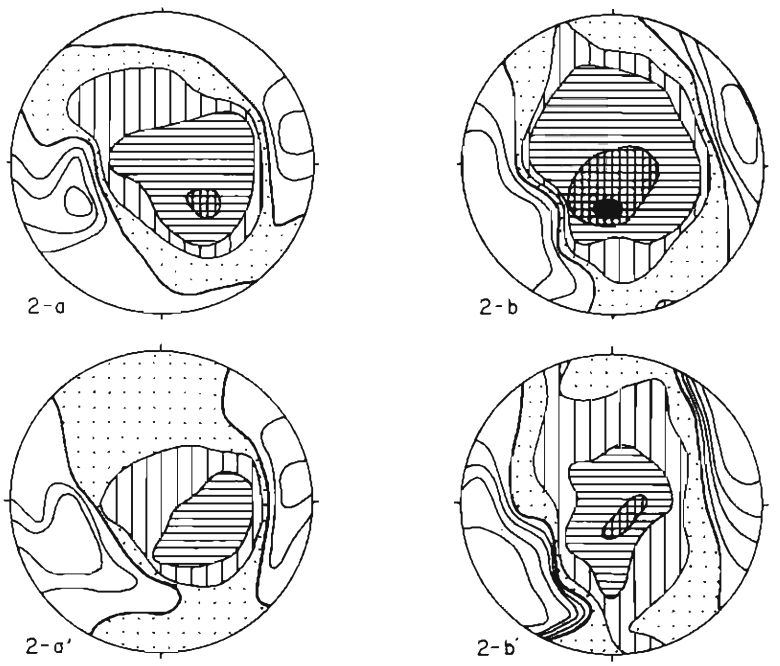

Fig. 9. (2-a): Chile, intermediate, and (2-b): Argentina, deep, 1964-1969. (2-a') and (2-b'): same regions, 1964-1965.

But there are two particular cases. One is that the axis of maximum tension of intermediate earthquakes in the Chile-Peru border region (3-c) has the same orientation as the axis of maximum pressure in the other regions. The other is that the axis of maximum pressure of intermediate earthquakes in the Colombia region (3-h) lies nearly horizontally in the NW-SE direction while it lies nearly vertically in the other regions.

The distribution of epicenters and the solutions in South America are shown in Fig. 11. The fault plane solutions of eight individual earthquakes coincide with the smoothed radiation patterns well. But in this region the distribution of the observation stations is biased in the north-south direction, and so the accuracy of the normalized parameter k is more or less unequally distributed. The number of initial data in each region, however, is sufficiently large to determine the principal axes of stress, so the results are considered to be reliable.

Santô (1969) studied the characteristics of seismicity in South America and pointed out the seismic activity of intermediate earthquakes is quite predominant in frequency.[12] The distribution of foci of intermediate earthquakes in Colombia which occurred in the nest N1 named in his paper extends in the NW-SE direction dipping toward inland. It is very interesting that the direction of the axis of maximum pressure in the same region (3-h) coincides well with the

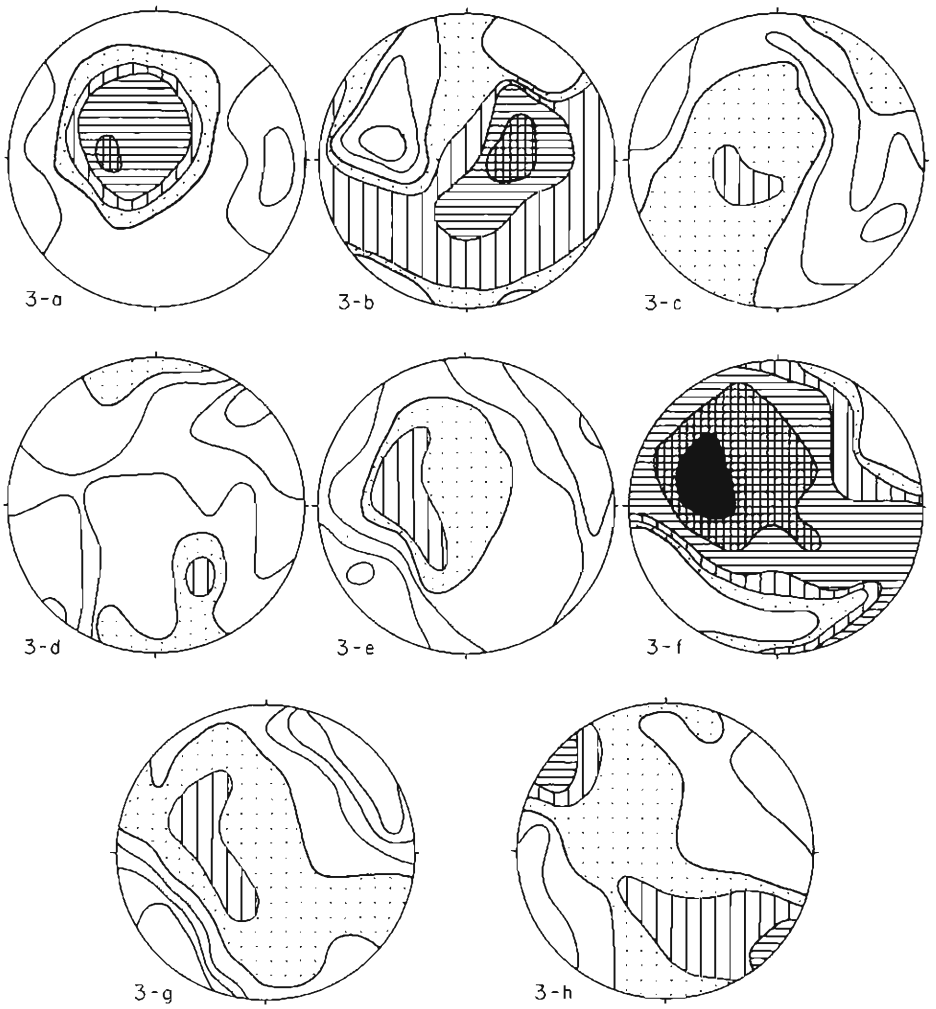

Fig. 10. (3-a): northern Chile, intermediate, (3-b): Bolivia, deep, (3-c): Peru-Chile border, intermediate, (3-d): Southern Peru, intermediate, (3-e): northern Peru, intermediate, (3-f): Brazil, deep, (3-g): Ecuador, intermediate, and (3-h): Colombia, intermediate.

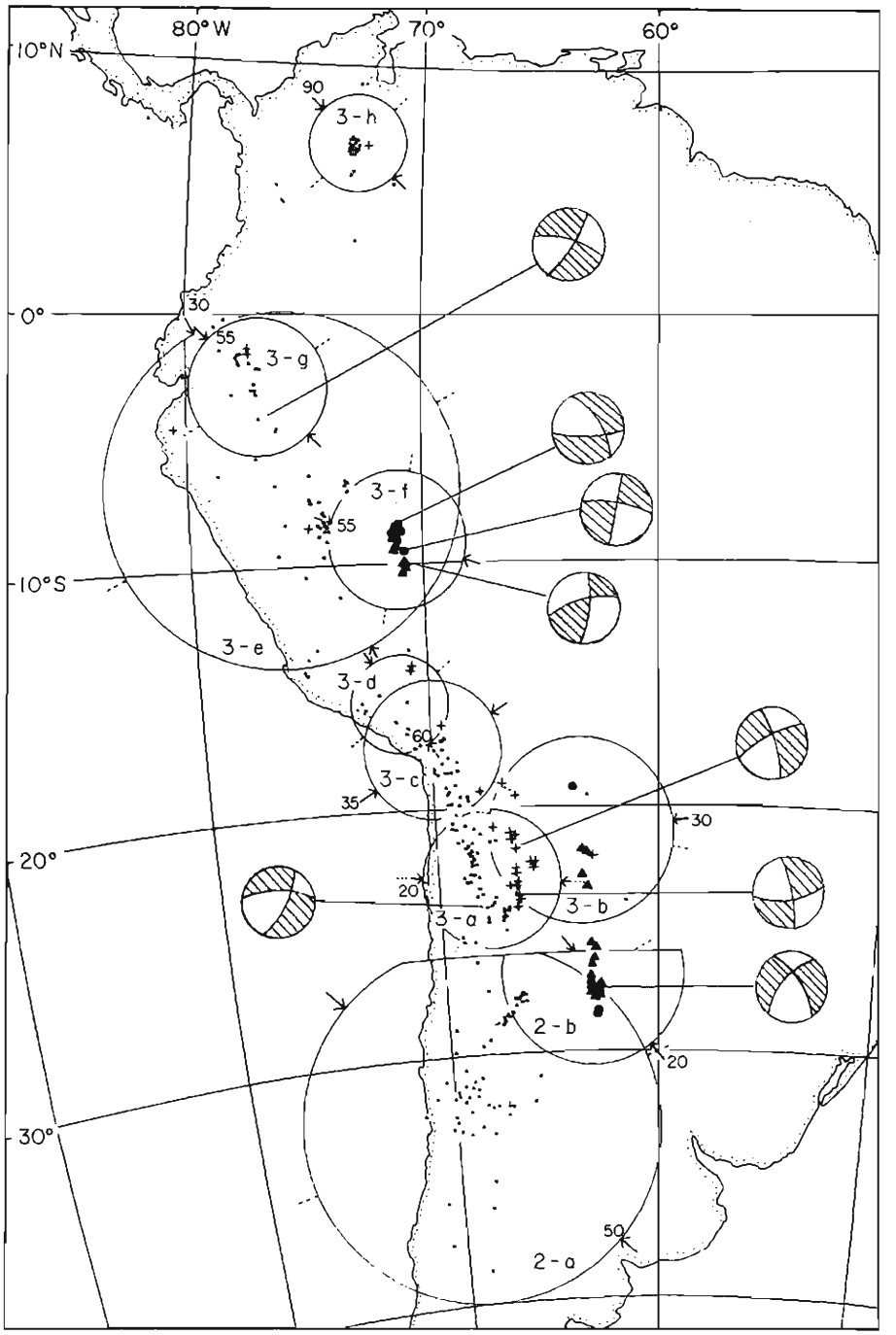

Fig. 11. Epicenter distribution and results for the South America region. Fault plane solutions of eight individual earthquakes are also shown as the projection of lower hemi-sphere.

direction of the distribution of foci.

c). Central America and West Indies.

The smoothed radiation patterns of the intermediate earthquakes in these regions are shown in Figs. 12 and 13. In the (4-c) and (5-a) regions the dilatational P motions are scarcely obtained because the observation stations are distributed in biased directions. Considering that the axis of maximum pressure in these two regions also coincides with the direction of the maximum k value, then the axes of maximum pressure in these regions lies nearly in the north-south direction except that the axis of pressure of (4-b) is nearly vertical. No. 4688 earthquake in Fig. 37 shows also the same pattern as the (5-a) region. The distribution of epicenters and the principal axes are shown in Figs. 14 and 15.

The patterns of (4-a) and (4-b) regions show the large value of maximum k and the results are reliable, but the directions of the axes of maximum pressure clearly differ from each other. It seems that this difference is related to the complex features of the seismic belt in these regions.

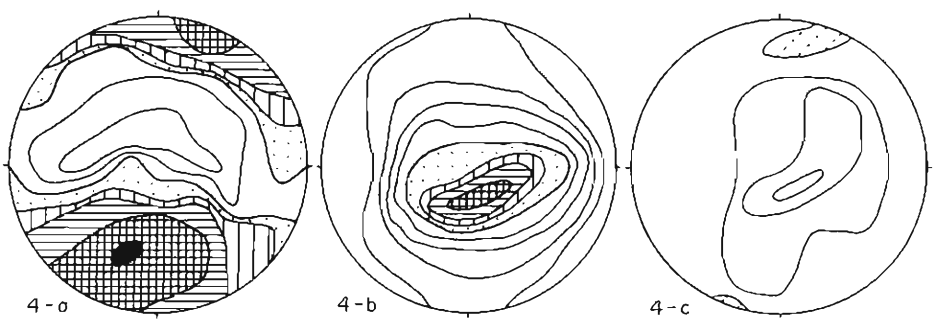

Fig. 12. (4-a): Trinidad Tobago, intermediate, (4-b): Leeward Islands, intermediate, and (4-c): Puerto Rico, intermediate.

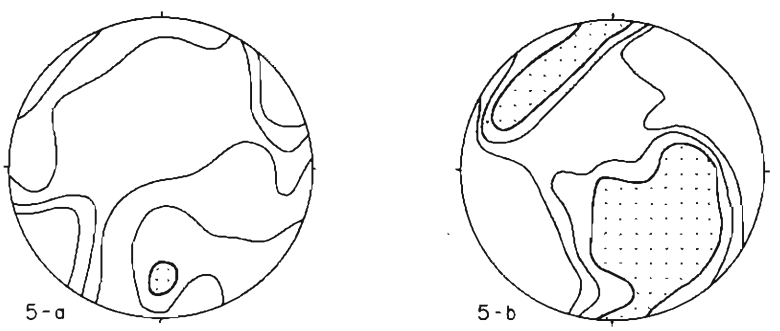

Fig. 13. (5-a): Guatemala-Nicaragua, intermediate, and (5-b): Mexico, intermediate.

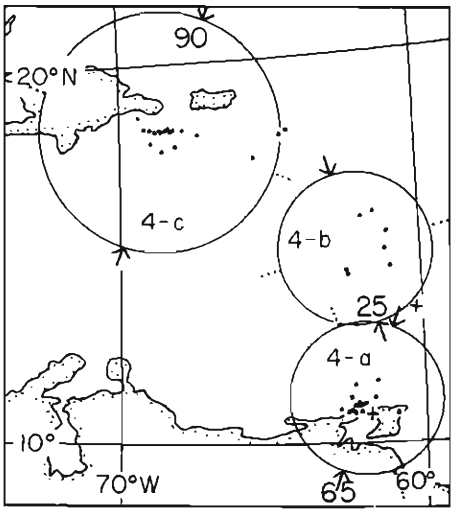

Fig. 14. Epicenter distribution and results for the West Indies region.

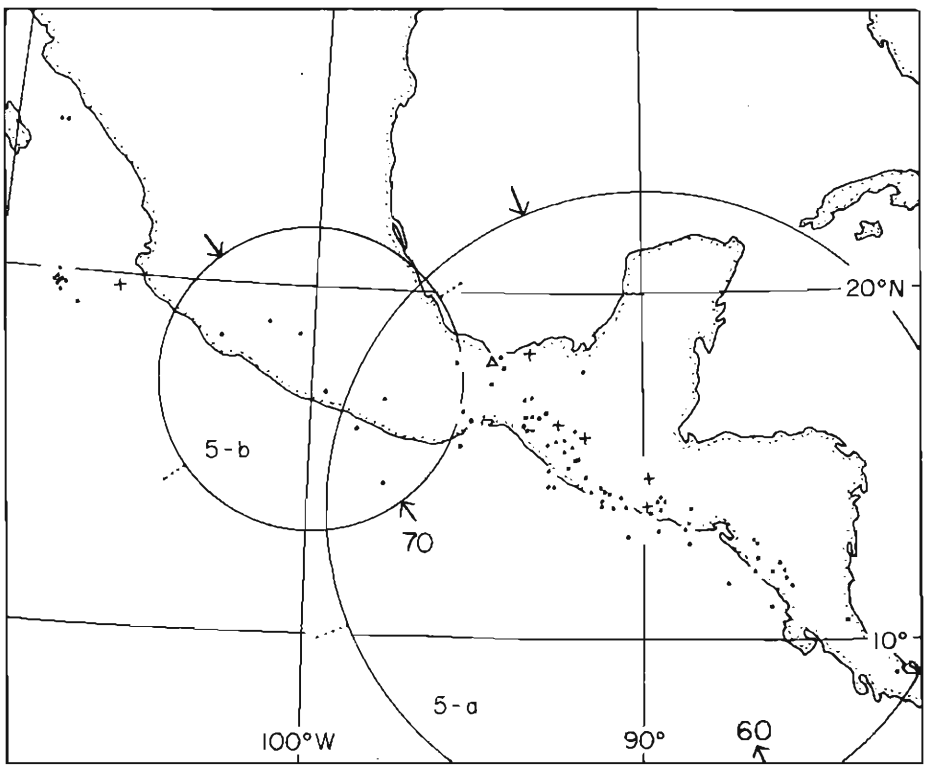

Fig. 15. Epicenter distribution and results for the Central America region.

d). *Alaska and Aleutian Islands.*

The results are shown in Figs. 16 and 17. The axis of maximum pressure lies in the NW-SE direction. It agrees well with the focal mechanism for shallow earthquakes occurring with the interior of the arc obtained by Stauder (1968),[13] who investigated the focal mechanism of shallow earthquakes in this region with relation to the sea-floor spreading.

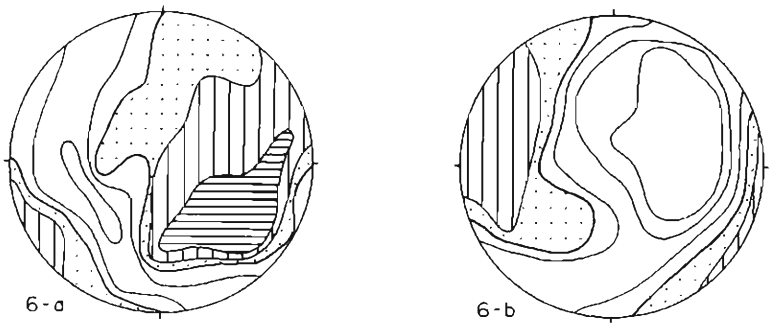

Fig. 16. (6-a): Alaska, intermediate, and (6-b): Aleutian Islands, intermediate.

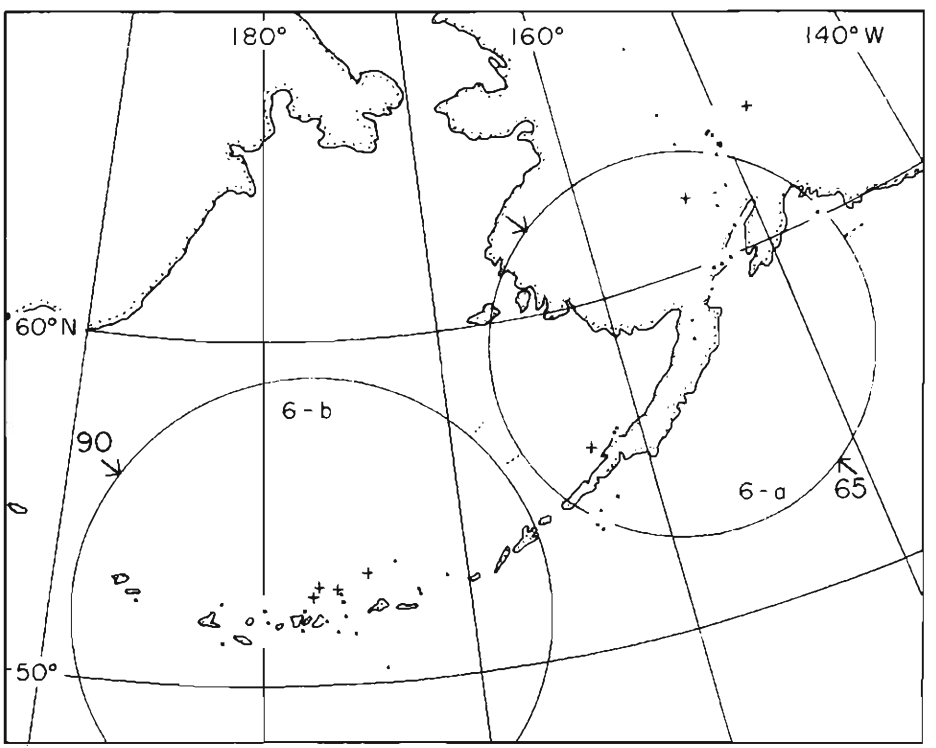

Fig. 17. Alaska and Aleutian Islands.

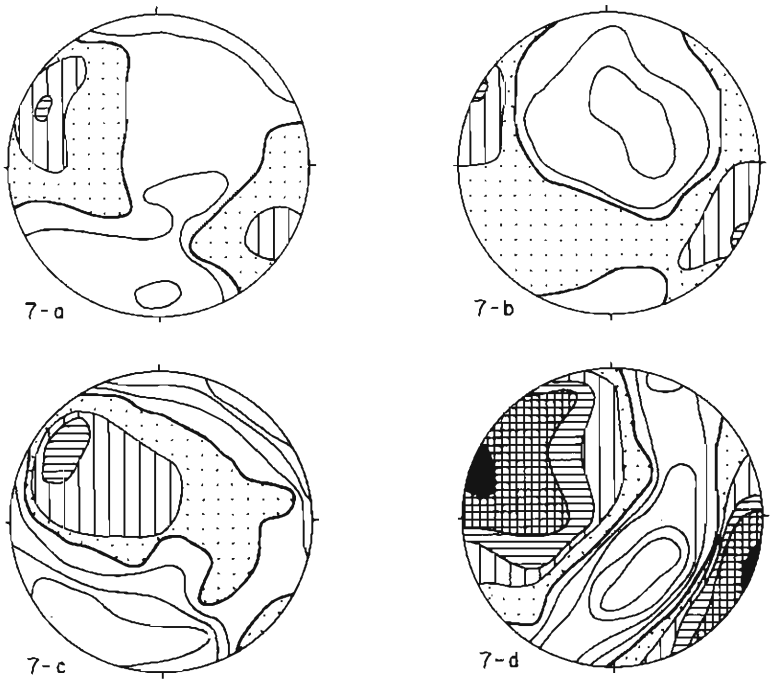

Fig. 18. (7-a): Kuril-Hokkaido of Japan (depth; 100-501 km), (7-b): Kuril-Hokkaido of Japan (depth; 100-289 km), (7-c): Kuril-Hokkaido of Japan (depth; 309-501 km), and (7-d): Japan Sea, deep.

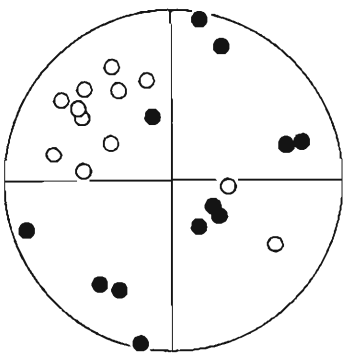

Fig. 19. Plots of P and T axes of individual solutions in Fig. 37 on the lower hemisphere projected by Wulf's net in the Kuril-Japan region.

e). *Kuril-Japan.*

The earthquake generating stress in this region has been investigated in detail for a long time, using the data supplied by the network of the Japan Meteorological Agency. Fig. 18 and a part of Fig. 20 (8-a, b and c) show results in this region for two years.

The direction of the axes of principal stress determined here from short-term data agrees well with the indications obtained by statistical analysis based on the fault plane solutions of individual earthquakes. Considering that our results are based on the smaller earthquakes (see Fig. 3), it seems that the axis of maximum pressure of earthquakes of various magnitude in the upper mantle lies constantly in the dipping direction of the seismic plane.

The epicenters of earthquakes in the regions

(7-a, b and c) are within the same region but they are classified with the depth of 100-501, 100-209 and 309-501 km, respectively. Their smoothed radiation patterns show similar results.

The pattern for deep earthquakes in Japan Sea region (7-d) show clearly that the variation of the k value is large and the directions of axes of maximum pressure and tension are constant for all earthquakes.

In the pattern for Honshu, in Japan, (8-a) the variation of the k value is very small in spite of the large amount of data. It is considered in terms of different groups of earthquakes with different directions of the principal axes. The patterns of (8-b and c) show the results obtained by classifing them into two groups. The axis of maximum pressure of the deeper group (8-c) lies in the same direction as the dip of the seismic plane. But in the shallower group (8-b) the axis of maximum tension lies nearly in the dipping direction of the

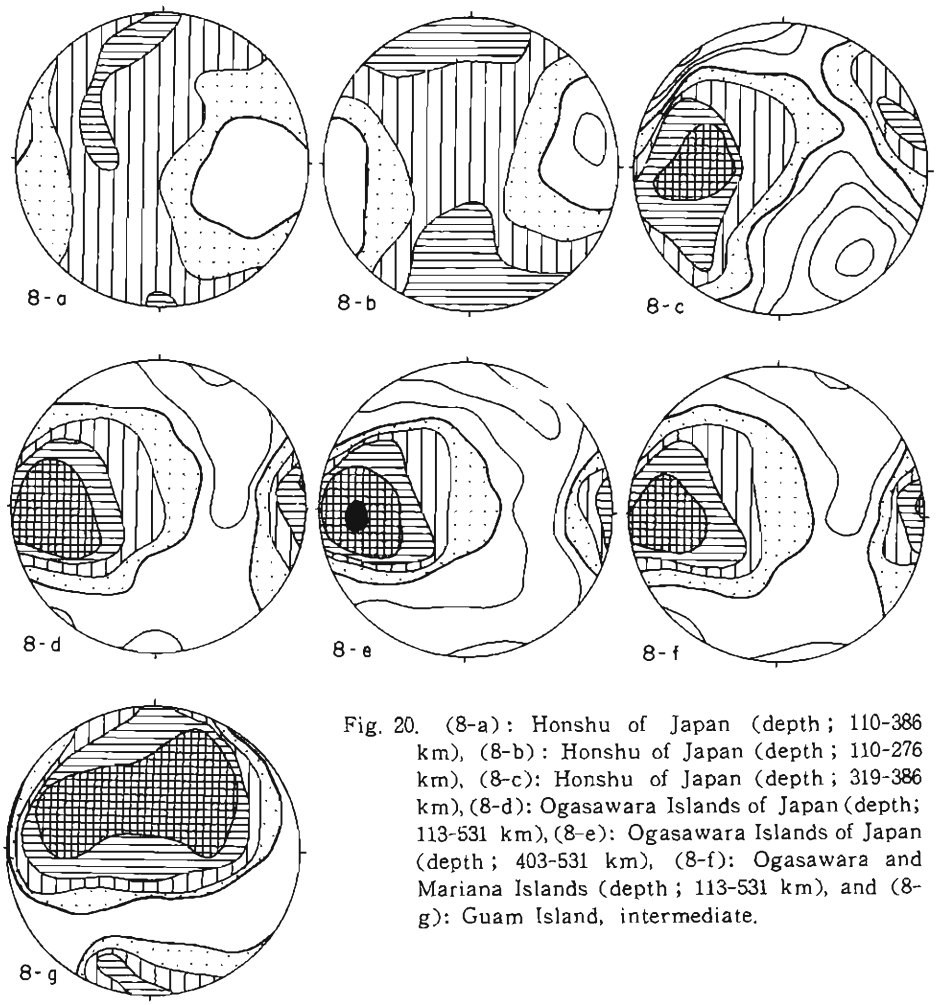

Fig. 20. (8-a): Honshu of Japan (depth; 110-386 km), (8-b): Honshu of Japan (depth; 110-276 km), (8-c): Honshu of Japan (depth; 319-386 km), (8-d): Ogasawara Islands of Japan (depth; 113-531 km), (8-e): Ogasawara Islands of Japan (depth; 403-531 km), (8-f): Ogasawara and Mariana Islands (depth; 113-531 km), and (8-g): Guam Island, intermediate.

seismic plane.

The axes of maximum pressure and tension obtained from the fault plane solutions of individual earthquakes in this region are plotted in Fig. 19. It shows the same pattern as the results obtained from the smoothed radiation patterns in this region.

f). *Izu-Mariana Islands.*

The results of investigations over two years are shown in Fig. 20 (8-d~g). The axis of maximum pressure in this region also lies in the direction of the dip of seismic plane. However, in Guam island the axis turns clockwise corresponding with curve of the island arc. These results agree with four fault plane solutions obtained by Katsumata and Sykes (1969),[14] and with our solutions shown in Fig. 21.

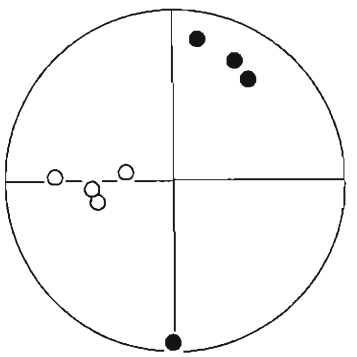

Fig. 21. Plots of P and T axes of individual solutions in the Izu-Mariana region.

The accuracy of the patterns is satisfactory because of a large amount of data and large value of the parameter *k*. It can be concluded that the axis of maximum pressure of earthquakes whose magnitudes are larger than about 4.0 lies nearly in the direction of the dip of the seismic plane.

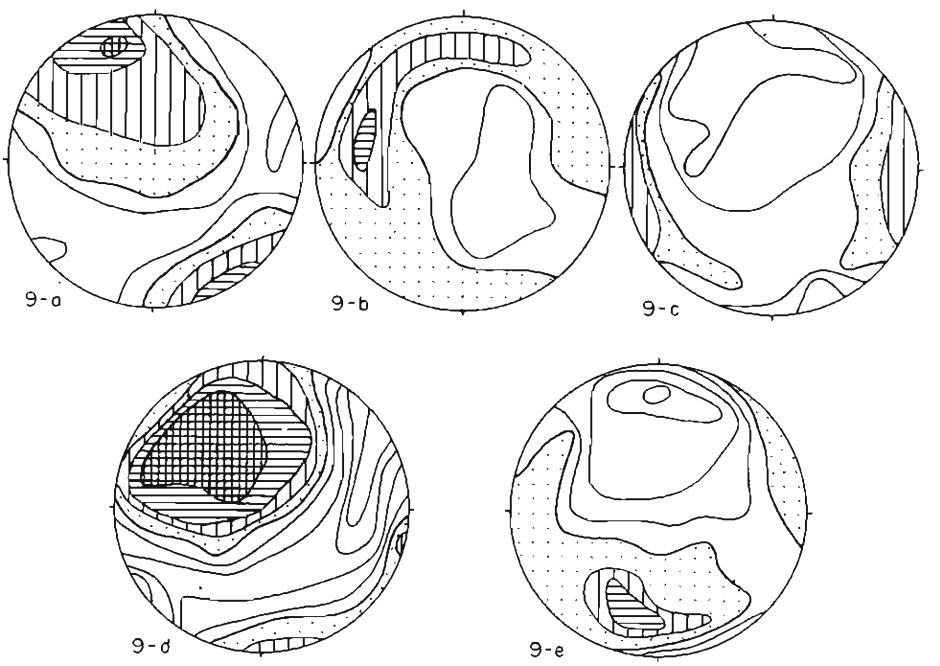

Fig. 22. (9-a): Nansei Islands, intermediate, (9-b): Taiwan-Philippines, intermediate, (9-c): Philippines, intermediate, (9-d): Philippines, deep, and (9-e): Celebes, intermediate.

g). *Ryukyu-Taiwan-Philippines.*

The results for the years 1964 to 1969 are shown in Fig. 22. In the Ryukyu Islands region the fault plane solutions have been obtained by Ichikawa (1966),[15] and Katsumata and Sykes (1969).[16] The axes determined from the smoothed radiation pattern from the data of nineteen earthquakes agree with their results and the solution of No. 2199 earthquake in Fig. 37.

The results for Taiwan (9-b) and the Philippines (9-c) regions show that the axis of maximum pressure lies in the dipping direction of the seismic plane. This coincides with the characteristics of shallow earthquakes in this region presented by Fitch (1970).[17]

The deep earthquakes of Mindanao have a different pattern (9-d), which is also seen in the fault plane solution of No. 1279 earthquake in Fig. 37. This region and the surrounding regions have complex features of seismological phenomena related to the complexity of the tectonic movement due to the Pacific Ocean, the Philippine, the Asian and the Indian Ocean-Australian plates. It is necessary to investigate in particular detail the locality of the stress field in this region.

h). *Burma-Indonesia.*

The resutls are shown in Fig. 23. Though the accuracy of the pattern of the Burma region (10-a) is not satisfactory, it is concluded that the axis of maximum pressure lies nearly horizontally in the north-south direction. This conclusion is also supported by the facts that fault plane solutions presented by

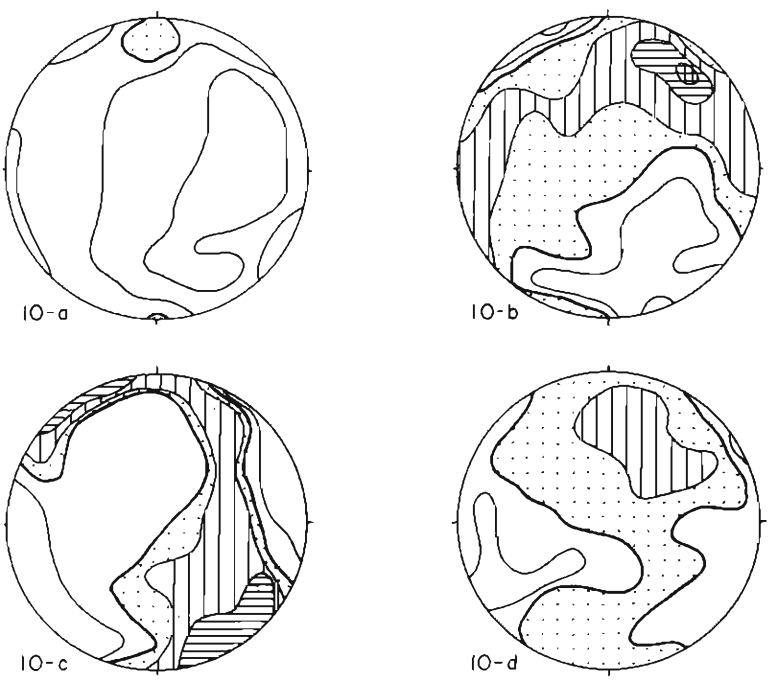

Fig. 23. (10-a): Burma, intermediate, (10-b): Sumatra, intermediate, (10-c): Java, intermediate, and (10-d): Banda Sea, intermediate and deep.

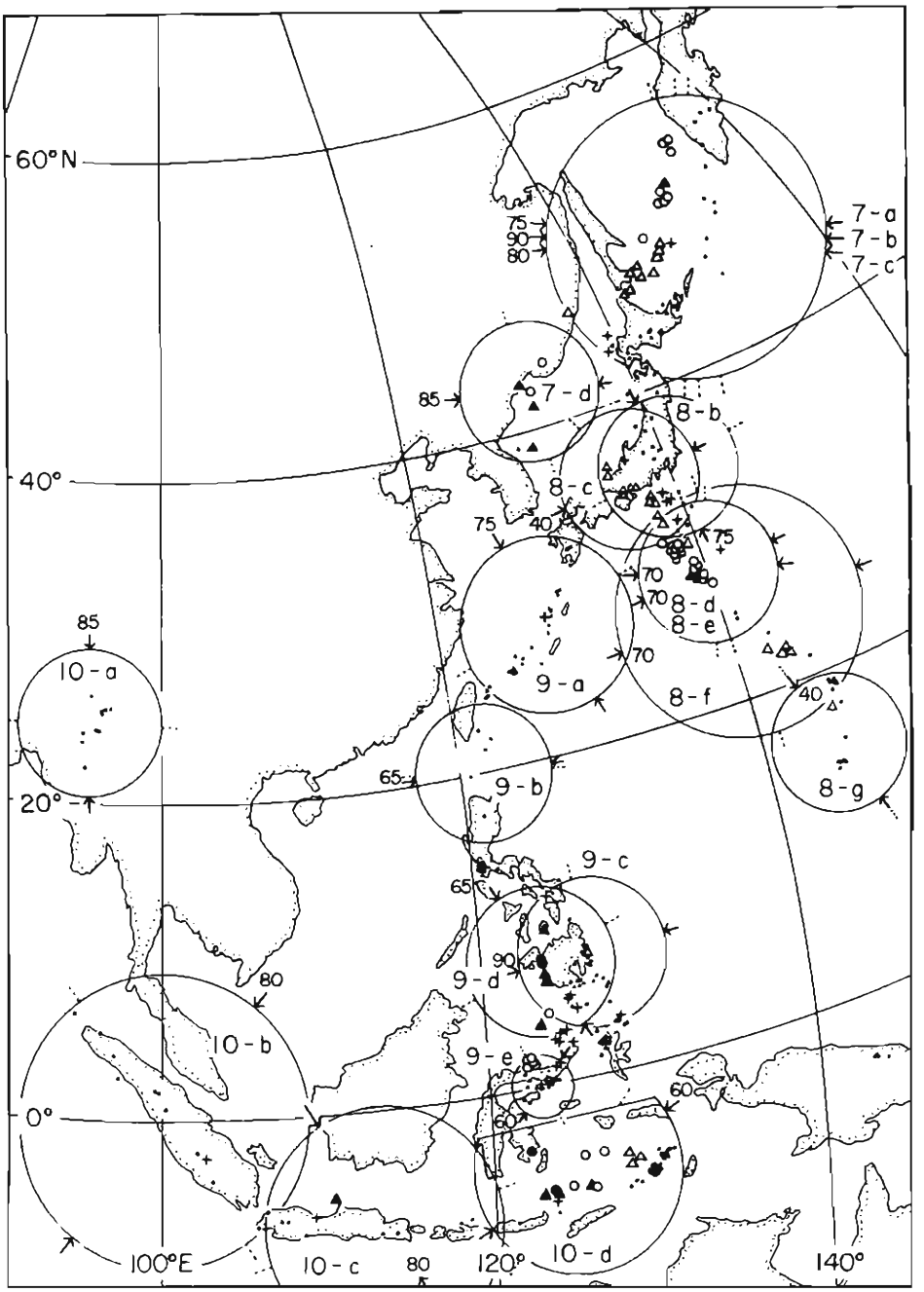

Fig. 24. Epicenter distribution and results for the No. 7~10 regions explained in sections e)~h).

Fitch (1970),[17] and a solution of No. 601 earthquake in Fig. 37 show the same characteristics.

The axes of maximum pressure of the Sumatra (10-b), the Java (10-c) and the Banda Sea (10-d) regions are shown to be perpendicular to the trend of the island arc and the trench. The fault plane solutions of deep earthquakes in the Banda Sea region (Nos. 263, 1068, 1212 and 2027 in Fig. 37) show complicated results corresponding to the complication of the structure of the seismic plane.

The orientations of the axes of intermediate earthquakes in the Indonesia region generally coincide with the results from the fault plane solutions of shallow earthquakes obtained by Fitch (1970).[17]

The distribution of the epicenters and the results explained in sections from e) to h) are shown in Fig. 24.

i). Solomom Islands and New Hebrides.

The smoothed radiation pattern of the Solomom Islands region is shown in Fig. 25 (11-a). The variation of the value of k is small, so the axis of maximum pressure cannot be determined clearly, but it seems that the axis lies perpendicular to the trend of the island arc. The plots of the P and T axes

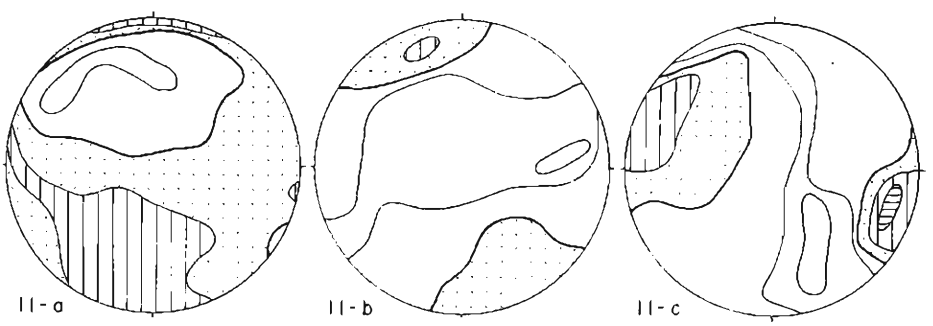

Fig. 25. (11-a): Solomon Islands, intermediate and deep, (11-b): New Hebrides, intermediate, and (11-c): Santa Cruz Islands, deep.

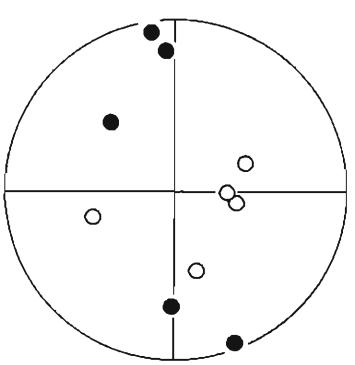

Fig. 26. Plots of P and T axes of individual solutions in the Solomon Islands region.

obtained from the fault plane solutions in this region are shown in Fig. 26. The P axes flock around the vertical. This seems to be related to the steep dip of the seismic plane of this region indicated by Denham (1969).[18]

The pattern of the New Hebrides area in Fig. 25 (11-b) shows that the axis of maximum pressure lies horizontally along the trend of the arc and the axis of maximum tension lies in the direction of dip of the seismic plane. The absolute value of minimum k is large compared with that of maximum k.

This means that the axes of maximum tension of all earthquakes lie in the same

direction. It is interesting that the direction of the axis of maximum tension in (11-b) corresponds to the direction of the axis of maximum pressure of deep earthquakes in the Santa Cruz Islands region (11-c). These characteristics are also found in the fault plane solutions shown in Fig. 37. The relation between the earthquake generating stress and the complicated structure of the seismic plane in this region must be investigated in detail.

j). *Fiji-Kermadec Islands and New Zealand.*

The patterns of the Fiji and Kermadec Islands region are shown in Fig. 27. The axis of maximum pressure was determined to lie in the dipping direction

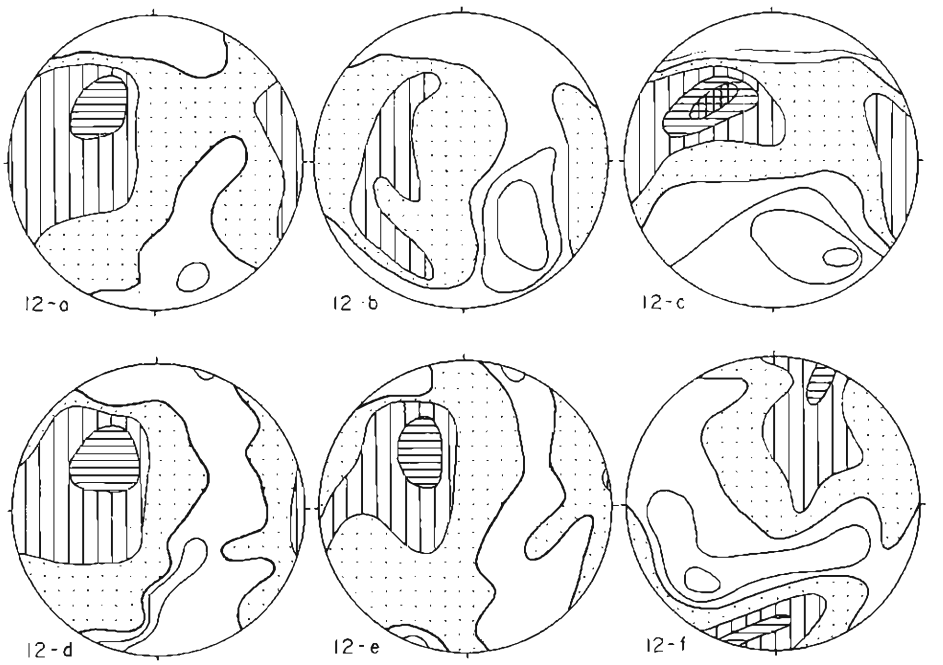

Fig. 27. (12-a): Fiji-Tonga-Kermadec, Deep, (12-b): Fiji, intermediate, (12-c): Fiji, deep, (12-d): Tonga, deep, (12-e): Tonga-Kermadec, deep, and (12-f): Kermadec, intermediate.

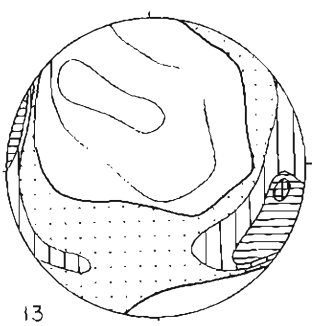

Fig. 28. New Zealand, intermediate.

of the seismic plane in each region. This coincides with the results obtained by Isacks et al. (1969),[19] and the fault plane solutions shown in Fig. 37. It seems that the direction of the axes in these regions is constant for time, space and magnitude.

The axis of maximum pressure in the New Zealand region shown in Fig. 28 lies nearly horizontally perpendicular to the trend of the arc. The same result is obtained from the fault plane solution of No. 2469 earthquake in Fig. 37.

The distribution of epicenters and the results

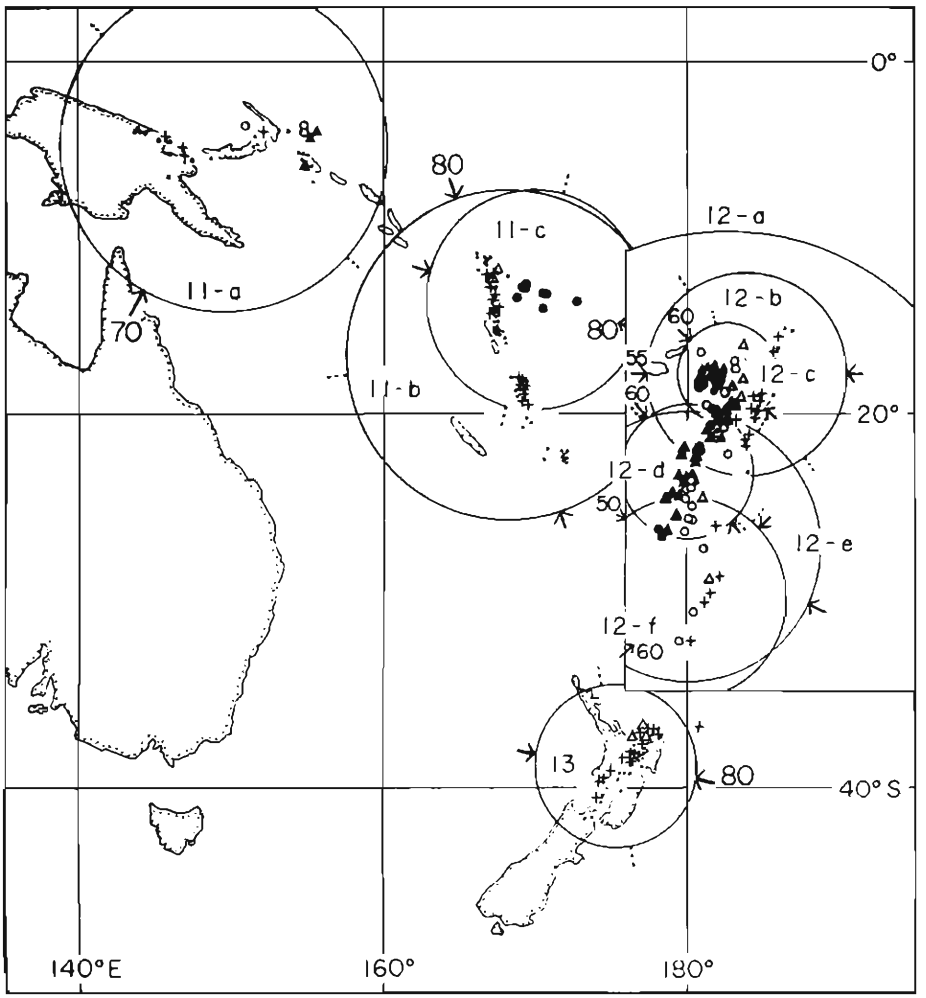

Fig. 29. Epicenter distribution and the results of No. 11~13 regions explained in sections of i) and j).

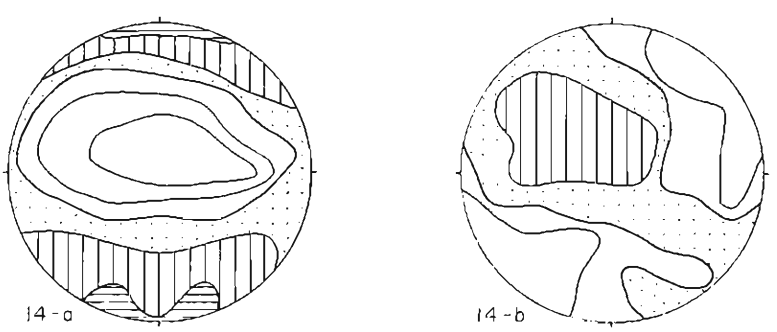

Fig. 30. Hindu-Kush, intermediate.

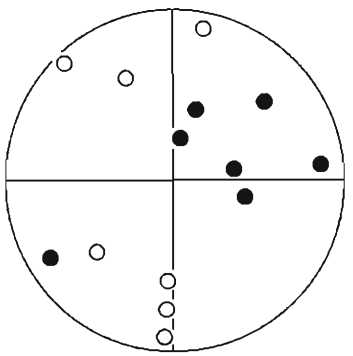

Fig. 31. Plots of P and T axes of individual solutions in the Afghanistan-U. S. S. R. border region.

explained in sections i) and j) are shown in Fig. 29.

k). *Afghanistan-U. S. S. R. border.*

The smoothed radiation patterns of the Afghanistan-U. S. S. R. border region are shown in Fig. 30. The axis of maximum pressure lies perpendicular to the trend of the seismic belt. The plots of the P and T axes are compared in Fig. 31. The fault plane solutions of two intermediate earthquakes presented by Soboleva (1967)show similar results.[30] The distribution of the epicenters and the results are shown in Fig. 32.

It seems that the orientation of the axis of maximum pressure is closely related to the trend of the seismic belt from the Himalayan mountain front to the Hindu-Kush also con-

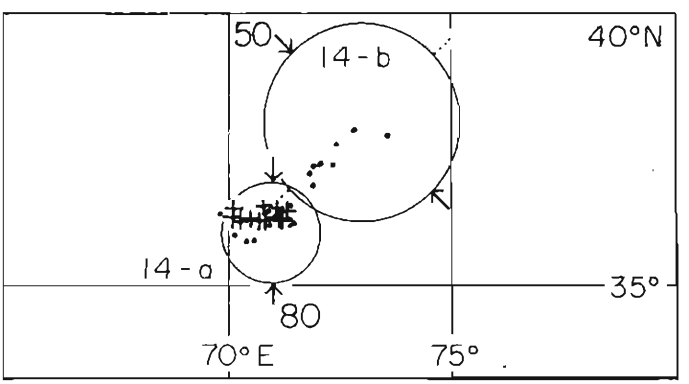

Fig. 32. Epicenter distribution and results for intermediate earthquakes in the Afghanistan-U. S. S. R. border region.

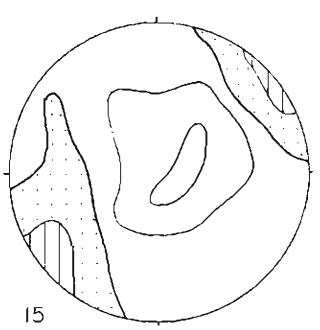

Fig. 33. Italy-Greece-Turkey, intermediate.

sidering the analyses of shallow earthquakes in this region obtained by Fitch (1970).[21]

l). *Italy-Greece-Turkey.*

The smoothed radiation pattern is shown in Fig. 33, and the distribution of epicenters and the results are shown in Fig. 34. Although the maximum value of the parameter k is not large, the axis of maximum pressure can be determined to be in the NE-SW direction. But the distribution of hypocenters is not sufficient to analyze the locality.

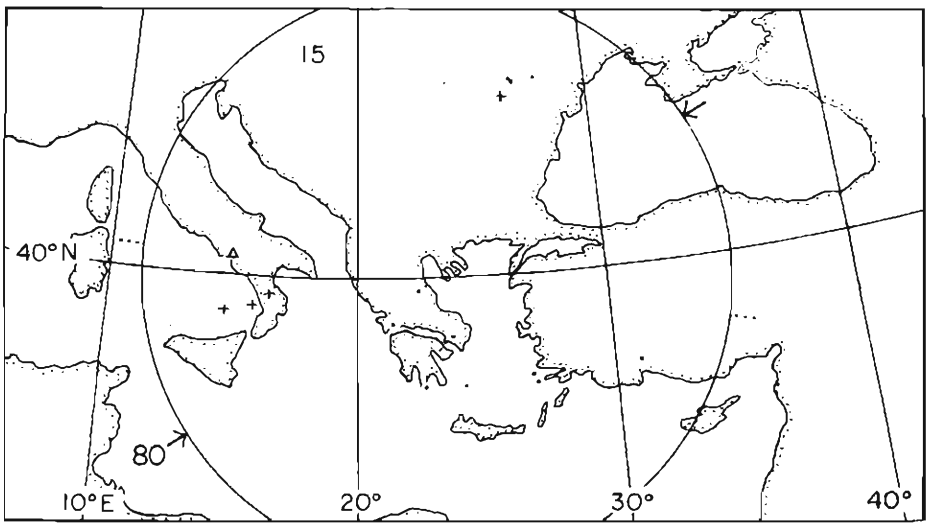

Fig. 34. Epicenter distribution and the results of the Italy-Greece-Turkey region.

5. Conclusions and Discussions.

In Fig. 35 the results for all regions are superposed on the world map of the distribution of computed rates of compression and dilatation along boundaries of six lithospheric blocks presented by Le Pichon (1968) from magnetic anomalies at sea and the orientation of oceanic fracture zones.[22] Comparing the direction of the horizontal component of the axis of maximum pressure determined from a smoothed radiation pattern in each region with the differential movement between two blocks calculated from non-seismic data, the following characteristics are found.

a). Generally the direction of the axis of maximum pressure in each region coincides well with the direction of the differential movement.

b). It seems that this direction is controlled by the block movement on a large scale and so the axis does not always lie perpendicular to the trend of the arc or the trench, as found for example in the Aleutian Islands region.

c). The horizontal component of the axes of maximum pressure of the South America region lie in the NW-SE direction, and their vectors lie nearly vertical, and so do not coincide so well with the direction of the vectors of differential movement in this region. It is necessary to investigate in detail the focal mechanism of earthquakes in this region.

d). In some regions the axis of maximum tension of intermediate earthquakes lies in the dipping direction of the seismic plane or perpendicular to the trend of the island arc as the axis of maximum pressure of surrounding regions lies in the same direction. A possible model explaining the mechanism of such phenomena has been presented by Savage (1969).[23] Such a region is closely connected with a region where the seismic activity of deep earthquakes is predominant, for example South America (3-c), Japan (7-b) and New Hebrides (11-b).

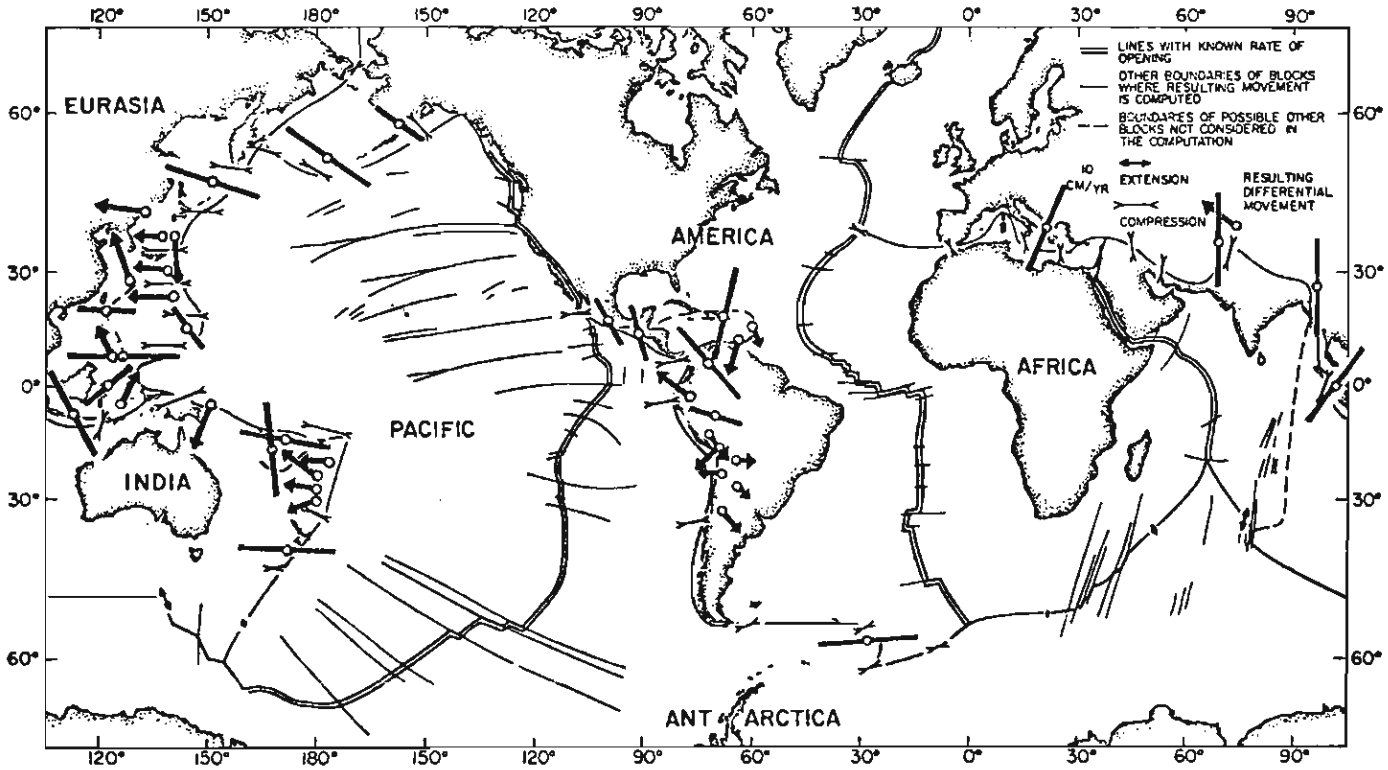

Fig. 35. Horizontal component of the axis of maximum pressure in each region compared with the vectors of the differential movement between two blocks computed by Le Pichon (1968). Heavy solid lines with arrow heads indicate the dipping direction of the axis of maximum pressure and those without arrow heads mean that the axis lies nearly horizontally.

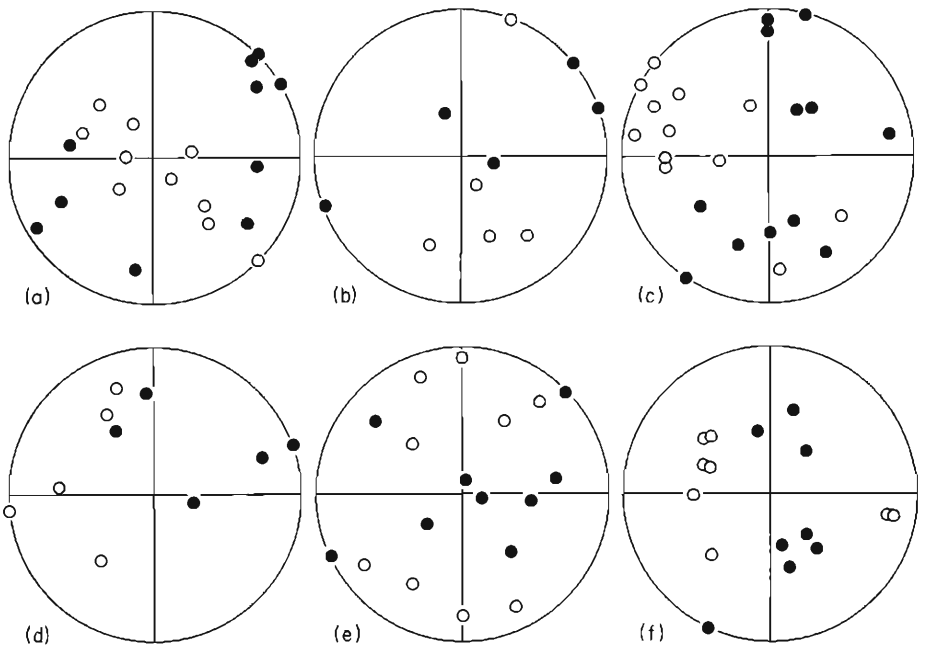

Fig. 36. Plots of P and T axes determined from the smoothed radiation patterns of six major boundaries between lithospheric blocks; (a): South America, (b): Central America, (c): North-West Pacific, (d): Philippine Sea, (e): northern edge of the Africa and India Plates, and (f): South-West Pacific. Filled and unfilled circles indicate T and P axes, respectively.

e). The stress field of the Central America, the Banda Sea and the New Hebrides region, where the structure of the seismic plane is complicated, also shows complicated features. It is necessary to examine the locality in detail according to the fault plane solutions of individual earthquakes.

The plots of the P axes and T axes from the smoothed radiation patterns are shown in Fig. 36, for six main active zones of intermediate and deep earthquakes. These zones are major boundaries of lithospheric blocks where the differential movement is largely compressional. The average direction of the axes of maximum pressure in each zone coincides with the direction of the vector of the differential movement of two blocks which are in contact with the zone.

These characteristics could be predicted by the new global tectonics and are now presented as evidence to support it. Moreover, the seismological research of the seismicity, the focal mechanism of the occurrence of individual earthquakes, the fault plane solutions of shallow earthquakes, and so on, must be developed. The smoothed radiation patterns have been used effectively for the purpose in this paper, and it will be useful for the investigation of the new global tectonics to analyze shallow earthquakes by a similar method.

Acknowledgment

The data on which this paper is based were obtained from the Bulletin of the International Seismological Center and the Earthquake Data Report of the U. S. Coast and Geodetic Survey. I am grateful to Drs. Yoshimichi Kishimoto and Takeshi Mikumo for critically reading the manuscript. My thanks are also due to Miss Yû Tsushima and Mrs. Ritsuko Koizumi for assistance in the analysis. Computations were made on a FACOM 230-60 at the Computation Center, Kyoto University.

References

1) Isacks, B., J. Oliver and L. R. Sykes : Seismology and the New Global Tectonics, J. Geophys. Res., Vol. 73, 1968, pp. 5855-5899.
2) Honda, H., A. Masatsuka and M. Ichikawa : On the Mechanism of Earthquakes and Stresses Producing Them in Japan and Its Vicinity (Third Paper), Geophys. Mag., Vol. 33, 1967, pp. 271-279.
3) Ichikawa, M.: Mechanism of Earthquakes in and near Japan, 1950-1962, Pap. Met. Geophys., Vol. 16, 1966. pp. 201-229.
4) Katsumata, M. and L. R. Sykes: Seismicity and Tectonics of the Western Pacific: Izu-Mariana-Caroline and Ryukyu-Taiwan Regions, J. Geophys. Res., Vol. 74, 1969, pp. 5923-5948.
5) Isacks, B., L. R. Sykes and J. Oliver: Focal Mechanisms of Deep and Shallow Earthquakes in the Tonga-Kermadec Region and the Tectonics of Island Arcs, Bull. Geol. Soc. Amer., Vol. 80, 1969, pp. 1443-1469.
6) Aki, K.: Earthquake Generating Stress in Japan for the Years 1961 to 1963 Obtained by Smoothing the First Motion Patterns, Bull. Earthq. Res. Inst., Vol. 44, 1966, pp. 447-471.
7) McKenzie, D. P.: The Relation between Fault Plane Solutions for Earthquakes and the Directions of the Principal Stresses, Bull. Seis. Soc. Amer., Vol. 59, 1969, pp. 591-601.
8) Barazangi, M. and J. Dorman: World Seismicity Maps Compiled from ESSA, Coast and Geodetic Survey, Epicenter Data, 1961-1967, Bull. Seis. Soc. Amer., Vol. 59, 1969, pp. 369-380.
9) Knopoff, L. and M. J. Randall : The Compensated Linear-Vector Dipole ; A Possible Mechanism for Deep Earthquakes, J. Geophys. Res., Vol. 75, 1970, pp. 4957-4963.
10) Randall, M. J. and L. Knopoff: The Mechanism at the Focus of Deep Earthquakes, J. Geophys. Res., Vol. 75, 1970, pp. 4965-4976.
11) loc. cit. 6).
12) Santô, T.: Characteristics of Seismicity in South America, Bull. Earthq. Res. Inst., Vol. 49, 1969, pp. 635-672.
13) Stauder, W.: Tensional Character of Earthquake Foci beneath the Aleutian Trench with Relation to Sea-Floor Spreading, J. Geophys. Res., Vol. 74, 1968, pp. 7693-7701.
14) loc. cit. 4).
15) loc. cit. 3).
16) loc. cit. 4).
17) Fitch, T. J.: Earthquake Mechanisms and Island Arc Tectonics in the Indonesian-Philippine Region, Bull. Seis. Soc. Amer., Vol. 60, 1970, pp. 565-591.
18) Denham, D. : Distribtion of Earthquakes in the New Guinea Solomon Islands Region, J. Geophys. Res., Vol. 74, 1969, pp. 4290-4299.

Table 3. List of regional data and results. Region numbers correspond to those in figures. Earthquakes in each region were adopted by the conditions that the hypocenters were within a cylinder with a center, a radius and a range of the depth. The rank (A, B and C) means the accuracy of the results besed on the total number of data and their distribution on a focal sphere.

No.	Center		Rad. (km)	Depth (km)	N_e	ΣN_P	P. Axis			T. Axis			Rank
	Lat. (deg)	Long. (deg)					max. k	θ (deg)	φ (deg)	min. k	θ (deg)	φ (deg)	
1	−56	−28	300	101−181	32	234	0.35	80	260	−0.50	90	170	C
2−a	−32	−69	700	102−183	48	172	0.60	50	135	−0.60	70	245	B
2−b	−27	−63	500	555−602	12	158	0.82	20	140	−0.70	85	240	B
3−a	−23	−68	300	103−283	55	768	0.60	20	275	−0.52	70	95	A
3−b	−21	−64	400	533−602	5	58	0.70	30	85	−0.53	60	280	C
3−c	−18	−70	300	100−212	32	414	0.34	35	230	−0.41	75	125	B
3−d	−16	−72	200	100−185	9	137	0.30	60	140	−0.69	85	45	C
3−e	− 7	−76	700	104−295	36	651	0.33	30	330	−0.63	90	60	B
3−f	− 9	−71	300	585−650	9	334	0.86	55	290	−0.18	75	190	C
3−g	− 3	−77	300	103−232	17	373	0.31	55	315	−0.69	80	55	B
3−h	7	−73	200	109−209	25	412	0.44	90	135	−0.22	90	45	B
4−a	11	−62	200	100−215	14	88	0.80	65	200	−0.53	35	340	B
4−b	15	−62	200	100−173	5	22	0.65	25	160	−0.82	90	70	B
4−c	18	−69	300	103−181	14	124	−0.14	90	20	−0.79	25	110	C
5−a	14	−90	1,000	100−306	62	621	0.14	60	160	−0.90	90	70	C
5−b	17	−100	500	105−161	8	31	0.17	70	140	−0.50	90	50	C
6−a	58	−157	600	100−217	15	79	0.56	65	130	−0.59	60	235	C
6−b	52	−178	700	115−243	19	128	0.43	90	310	−0.79	45	40	C
7−a	49	150	1,000	100−501	34	1,538	0.40	80	295	−0.41	65	200	B
7−b	49	150	1,000	100−289	29	775	0.40	90	300	−0.47	40	30	A
7−c	49	150	1,000	309−501	19	753	0.53	75	305	−0.74	90	215	A
7−d	42	131	500	422−554	5	215	0.80	85	280	−0.89	50	180	A
8−a	35	140	500	110−386	25	998	0.45	65	315	−0.12	45	80	B
8−b	35	140	500	110−276	15	666	0.55	75	175	−0.29	80	80	B
8−c	35	137	400	319−386	10	330	0.71	40	265	−0.85	75	150	A
8−d	28	140	500	113−531	27	1,070	0.78	70	285	−0.40	90	15	B
8−e	28	140	500	403−531	19	783	0.81	70	265	−0.45	80	0	A
8−f	25	141	800	113−531	35	1,250	0.78	70	270	−0.33	85	0	B
8−g	15	145	500	101−332	15	340	0.78	40	340	−0.08	50	160	C

Table 3.

No.	Center		Rad. (km)	Depth (km)	N_e	ΣN_P	P. Axis			T. Axis			Rank
	Lat.	Long.					max. k	θ	φ	min. k	θ	φ	
9—a	28	128	600	102—250	19	460	0.63	75	340	—0.46	90	70	A
9—b	20	121	500	101—148	4	67	0.50	65	275	—0.35	30	100	C
9—c	8	127	500	100—375	25	444	0.30	90	265	—0.52	70	355	C
9—d	8	124	500	479—628	7	158	0.73	65	330	—0.82	75	70	B
9—e	0	123	200	108—212	19	341	0.55	60	220	—0.81	55	330	C
10—a	25	95	500	101—158	9	198	0.19	85	0	—0.52	50	95	C
10—b	0	100	1,000	104—203	13	220	0.60	80	40	—0.50	55	140	B
10—c	—8	114	800	112—524	8	160	0.56	80	155	—0.33	90	245	B
10—d	—6	125	700	112—605	12	128	0.36	60	30	—0.34	35	230	B
11—a	— 5	150	1,000	101—512	33	601	0.31	70	210	—0.24	75	310	B
11—b	—17	168	1,000	100—271	59	633	0.20	80	340	—0.40	65	80	B
11—c	—14	170	700	325—658	11	179	0.46	80	110	—0.54	60	15	B
12—a	—25	178	1,500	304—651	93	1,839	0.51	50	295	—0.20	55	165	B
12—b	—18	—176	600	129—298	17	317	0.37	55	270	—0.50	50	140	C
12—c	—18	—177	300	306—498	10	250	0.69	60	315	—0.60	40	165	A
12—d	—23	180	400	431—630	50	936	0.52	60	315	—0.26	40	140	B
12—e	—27	180	800	401—627	50	930	0.47	50	295	—0.22	90	205	B
12—f	—30	180	600	205—304	6	98	0.50	60	225	—0.50	40	40	C
13	—39	175	500	105—311	44	240	0.65	80	100	—0.49	45	350	B
14—a	36	71	100	103—279	43	871	0.47	80	180	—0.56	10	0	A
14—b	38	73	200	104—282	9	171	0.30	50	315	—0.29	90	45	C
15	40	23	1,000	105—310	16	243	0.26	80	235	—0.46	15	100	C

Table 4. List of earthquakes whose fault plane solutions are individually obtained and their results.

No.	Date	Lat. (deg)	Long. (deg)	Depth (km)	M	Reg.	P. Axis		T. Axis	
							θ (deg)	φ (deg)	θ (deg)	φ (deg)
462	May 26, 1964	−56.45	−27.70	114	5.8	1	80	50	52	143
2492	Dec. 13, 1965	−56.14	−27.76	153	5.2	1	88	94	39	186
1114	Dec. 9, 1964	−27.46	−63.23	578	5.8	2 - b	56	178	90	88
770	Sep. 6, 1964	−21.51	−66.77	232	4.8	3 - a	54	209	76	109
786	Sep. 11	−23.88	−66.63	195	5.1	3 - a	51	286	65	38
965	Nov. 2	− 4.04	−76.80	114	5.7	3 - e, g	51	259	77	158
1077	Nov. 28	− 7.90	−71.29	650	5.3	3 - f	41	331	57	199
1156	Dec. 22	− 9.48	−71.21	615	5.2	3 - f	72	144	74	229
1369	Feb. 18, 1965	− 9.99	−71.08	593	5.2	3 - f	90	140	50	230
1648	May 3	−24.27	−67.87	127	5.5	3 - a	37	233	86	138
4688	Feb. 3, 1968	16.59	−93.52	142	5.5	5 - a	57	169	68	274
72	Jan. 24, 1964	38.75	129.54	557	5.3	7	63	308	29	149
448	May 21	42.90	141.90	129	4.4	7 - a, b	68	333	26	120
1121	Dec. 11	38.90	130.22	551	5.1	7 - d	56	330	72	73
1979	Jul. 27, 1965	40.21	139.36	195	4.7	7	60	306	30	125
2006	Aug. 1	46.82	143.84	384	5.1	7 - a, c	73	306	63	207
2007	Aug. 1	52.73	153.48	446	5.0	7 - a, c	67	316	66	215
2022	Aug. 6	41.39	131.34	554	5.0	7 - d	64	283	76	20
2114	Sep. 1	51.29	150.70	501	5.1	7 - a, c	55	347	83	252
2325	Oct. 25	44.21	145.45	159	6.1	7 - a, b	63	122	36	348
407	May 7, 1964	30.59	137.84	485	5.3	8 - d, e, f	25	282	85	181
511	Jun. 11	33.10	137.89	341	4.8	8 - a, c	47	277	87	10
1402	Mar. 3, 1965	28.12	139.51	507	5.1	8 - d, e, f	42	255	70	18
1560	Apr. 12	30.21	138.68	425	5.5	8 - d, e, f	44	265	66	36
1637	May. 1	33.48	138.97	230	4.5	8 - a, b	38	302	63	72
1869	Jun. 23	35.51	135.56	363	5.0	8 - a, c	30	98	88	192
2078	Aug. 19	30.29	138.58	443	4.9	8 - d, e, f	63	273	76	10
596	Jul. 11, 1964	5.93	126.31	183	5.0	9 - c	82	338	48	75
1279	Jan. 23, 1965	7.43	123.86	628	5.2	9 - d	52	316	68	64
1569	Apr. 15	25.04	122.78	178	5.3	9	77	205	42	307
2199	Sep. 21	28.96	128.23	195	6.0	9 - a	53	340	85	246
2501	Dec. 15	0.00	123.69	164	5.3	9 - e	76	225	78	318
4264	Sep. 7, 1967	2.69	124.30	274	5.8	9	52	260	80	358
4761	Mar. 3, 1968	1.63	122.55	435	5.5	9	65	285	69	25

Table 4.

No.	Date	Lat. (deg)	Long. (deg)	Depth (km)	M	Reg.	P. Axis		T. Axis	
							θ	φ	θ	φ
263	Mar. 21, 1964	— 6.44	127.96	373	5.8	10-d	64	9	72	270
601	Jul. 12	24.88	95.31	152	5.5	10-a	64	219	76	122
1068	Nov. 25	— 4.34	122.14	607	5.8	10-d	90	160	62	70
1212	Jan. 6, 1965	— 7.13	122.84	554	5.3	10-d	90	290	90	20
2027	Aug. 9	— 6.99	123.32	605	4.8	10-d	60	18	62	270
585	Jul. 9, 1964	—15.56	167.62	127	6.4	11-b	73	275	24	48
755	Sep. 2	—18.56	169.31	223	4.7	11-b	66	120	83	217
1081	Nov. 29	—19.18	169.33	254	4.7	11-b	90	85	90	175
1313	Jan. 30, 1965	—13.05	169.58	644	4.9	11-c	84	59	8	180
1407	Mar. 4	— 5.46	147.00	191	5.6	11-a	45	252	86	158
1551	Apr. 10	—13.45	170.30	641	5.3	11-c	67	306	74	43
1913	Jul. 6	— 4.48	155.07	509	5.6	11-a	33	110	75	356
2152	Sep. 12	—11.25	166.36	130	5.1	11-b	77	150	13	330
2429	Nov. 25	— 4.00	150.54	460	5.2	11-a	44	165	50	316
2466	Dec. 7	— 6.39	146.31	118	5.9	11-a	40	68	71	182
2478	Dec. 11	— 4.42	154.98	512	5.1	11-a	28	90	85	351
482	May 29, 1964	—26.11	178.30	617	4.8	12-a, d, e	90	110	90	20
514	Jun. 12	—26.53	178.57	600	5.0	12-a, e	78	358	70	264
579	Jul. 7	—23.58	—179.83	462	5.3	12-a, d, e	88	175	87	85
617	Jul. 17	—24.34	179.52	504	4.8	12-a, d, e	57	214	56	98
744	Aug. 28	—19.85	—178.15	576	4.9	12-a, d	45	268	62	145
831	Sep. 21	—21.96	—179.46	603	5.2	12-a, d, e	40	298	64	72
1440	Mar. 13, 1965	—20.43	—177.63	502	5.1	12-a, d, e	48	215	67	114
1540	Apr. 7	—21.04	—178.80	591	4.9	12-a, d, e	15	300	75	130
1543	Apr. 8	—17.72	—178.58	565	5.3	12-a	55	220	51	95
1716	May 19	—20.85	—178.41	499	5.1	12-a, d, e	28	8	65	160
1772	Jun. 2	—23.53	179.99	538	5.4	12-a, d, e	90	135	0	0
2177	Sep. 17	—23.31	179.27	566	5.1	12-a, d, e	45	318	45	140
2349	Nov. 1	—24.18	179.02	550	5.3	12-a, d, e	45	260	58	132
2473	Dec. 9	—18.12	—178.12	649	5.4	12-a	35	45	67	172
2469	Dec. 8, 1965	—37.03	177.52	153	5.6	13	64	145	29	295
145	Feb. 18, 1964	36.47	70.70	202	4.9	14-a	52	183	78	84
272	Mar. 23	38.27	73.65	130	5.2	14-b	60	335	78	238
1442	Mar. 14, 1965	36.42	70.73	205	6.4	14-a	67	184	23	10
1751	May 28	36.73	70.04	282	4.7	14-b	81	184	33	80
1815	Jun. 10	36.44	70.54	205	4.6	14-a	84	316	64	49
2164	Sep. 14	36.49	70.14	232	4.6	14-a	82	12	39	112
2305	Oct. 21	36.50	69.77	164	4.7	14	55	228	39	18

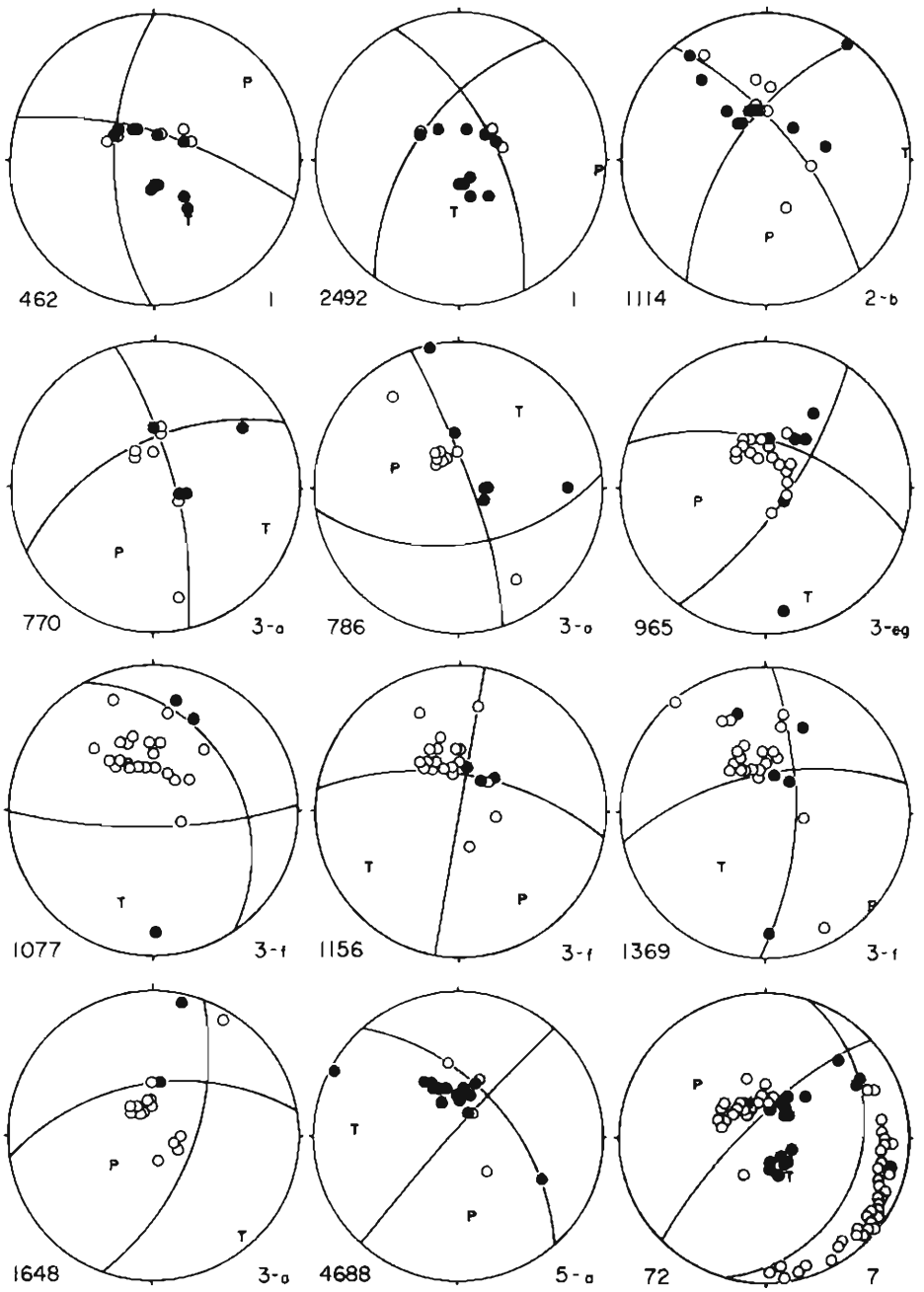

Fig. 37-a. Fault plane solutions and the first motion data in the form of the Wulf's net projection of lower hemi-sphere. Filled and unfilled circles indicate the compressions and the dilatations, respectively.

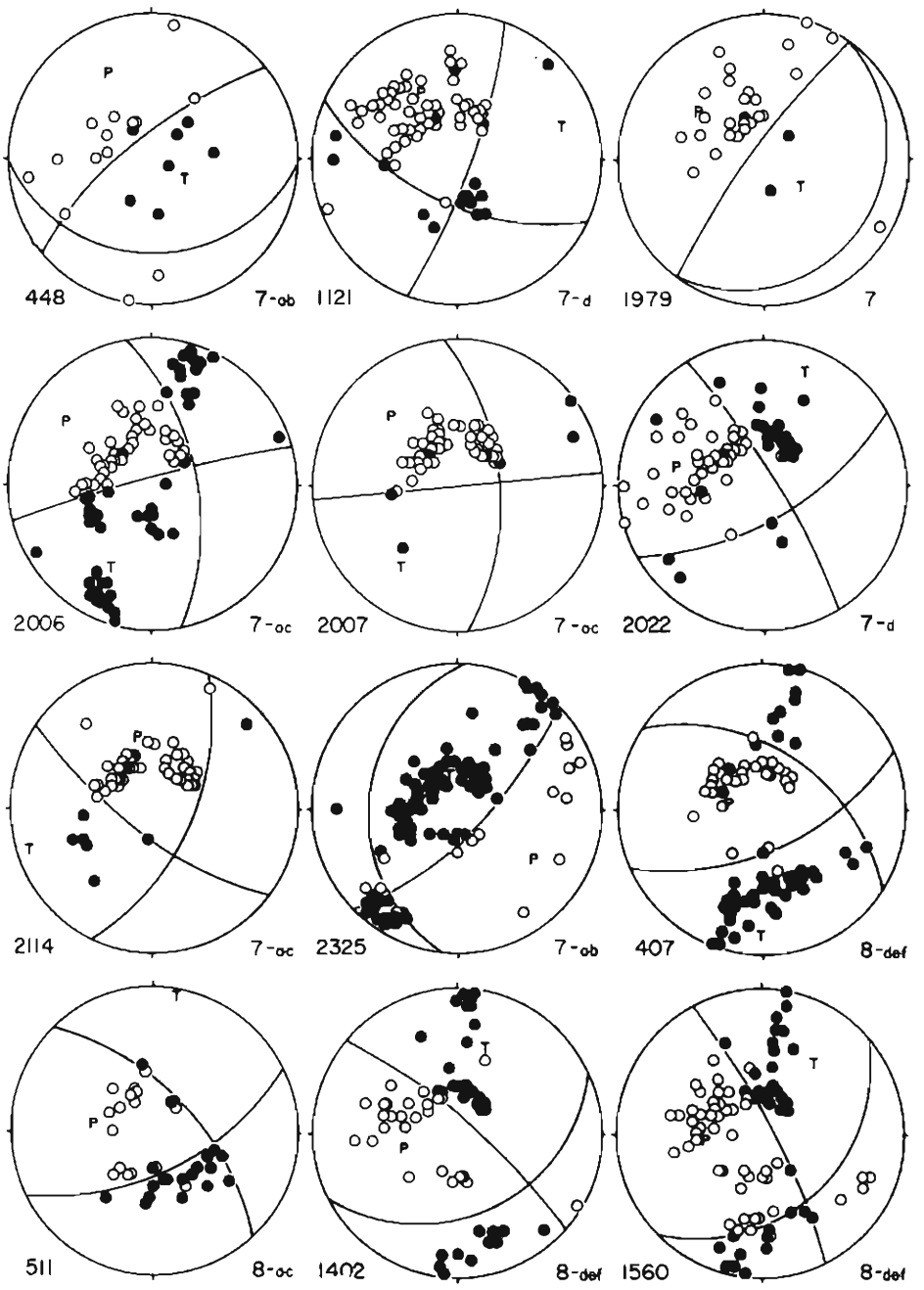
P
T
448
7-ab
1121
7-d
1979
7
2006
7-ac
2007
7-ac
2022
7-d
2114
7-ac
2325
7-ab
407
8-def
511
8-ac
1402
8-def
1560
8-def

Fig. 37-b.

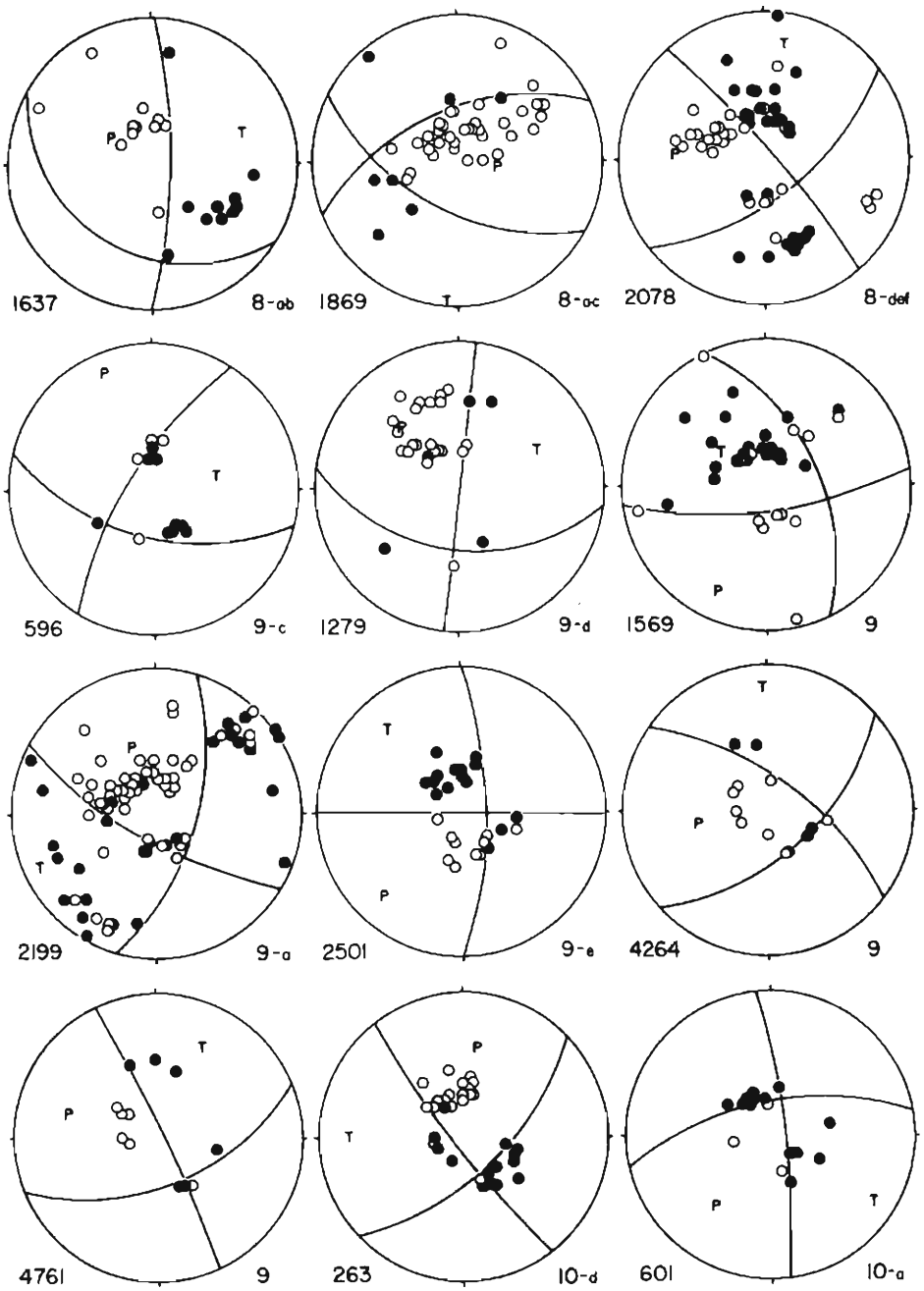
1637
8-ab
1869
8-ac
2078
8-def
596
9-c
1279
9-d
1569
9
2199
9-a
2501
9-e
4264
9
4761
9
263
10-d
601
10-a

Fig. 37-c.

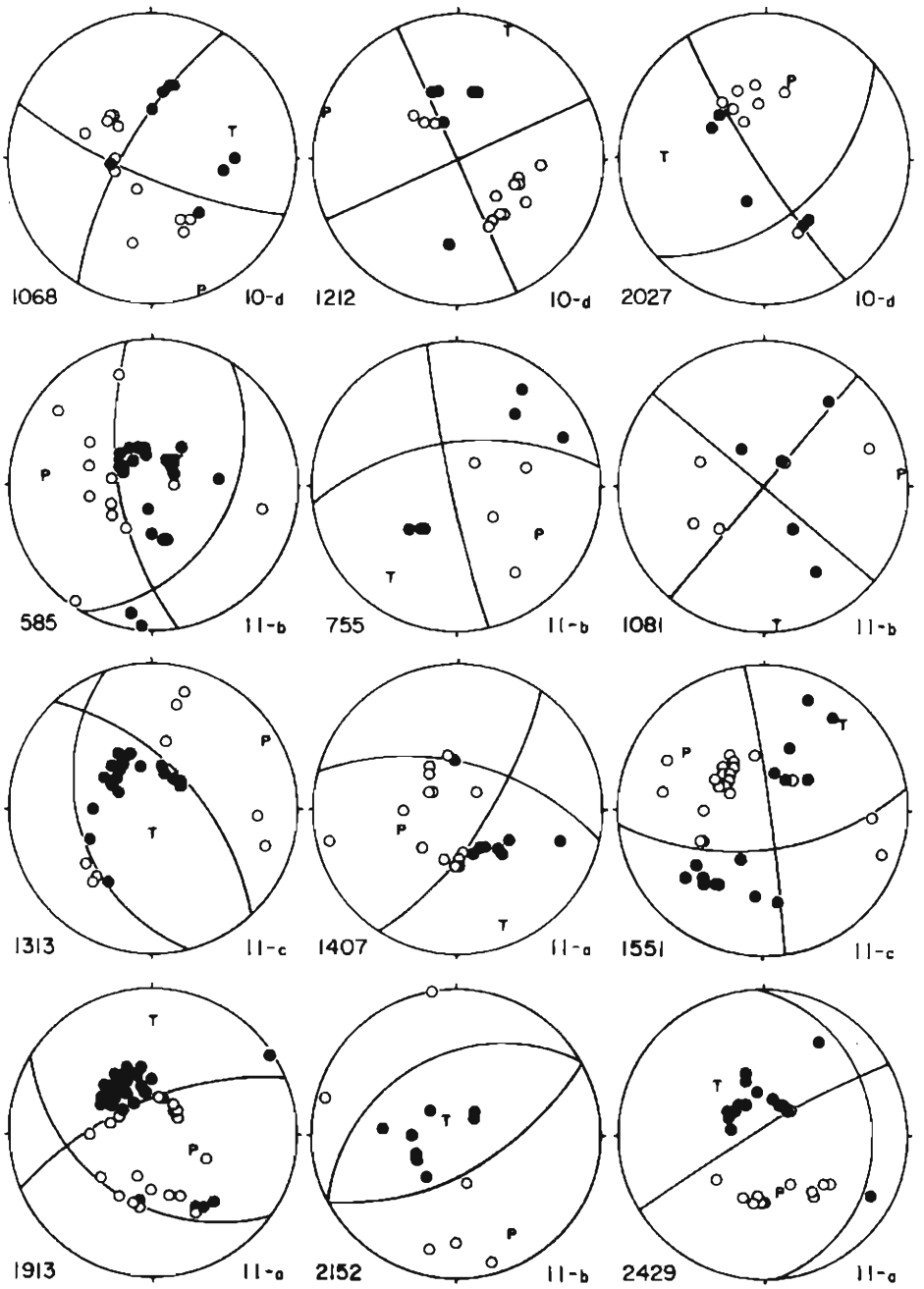
1068
10-d
1212
10-d
2027
10-d
585
11-b
755
11-b
1081
11-b
1313
11-c
1407
11-a
1551
11-c
1913
11-a
2152
11-b
2429
11-a

Fig. 37-d.

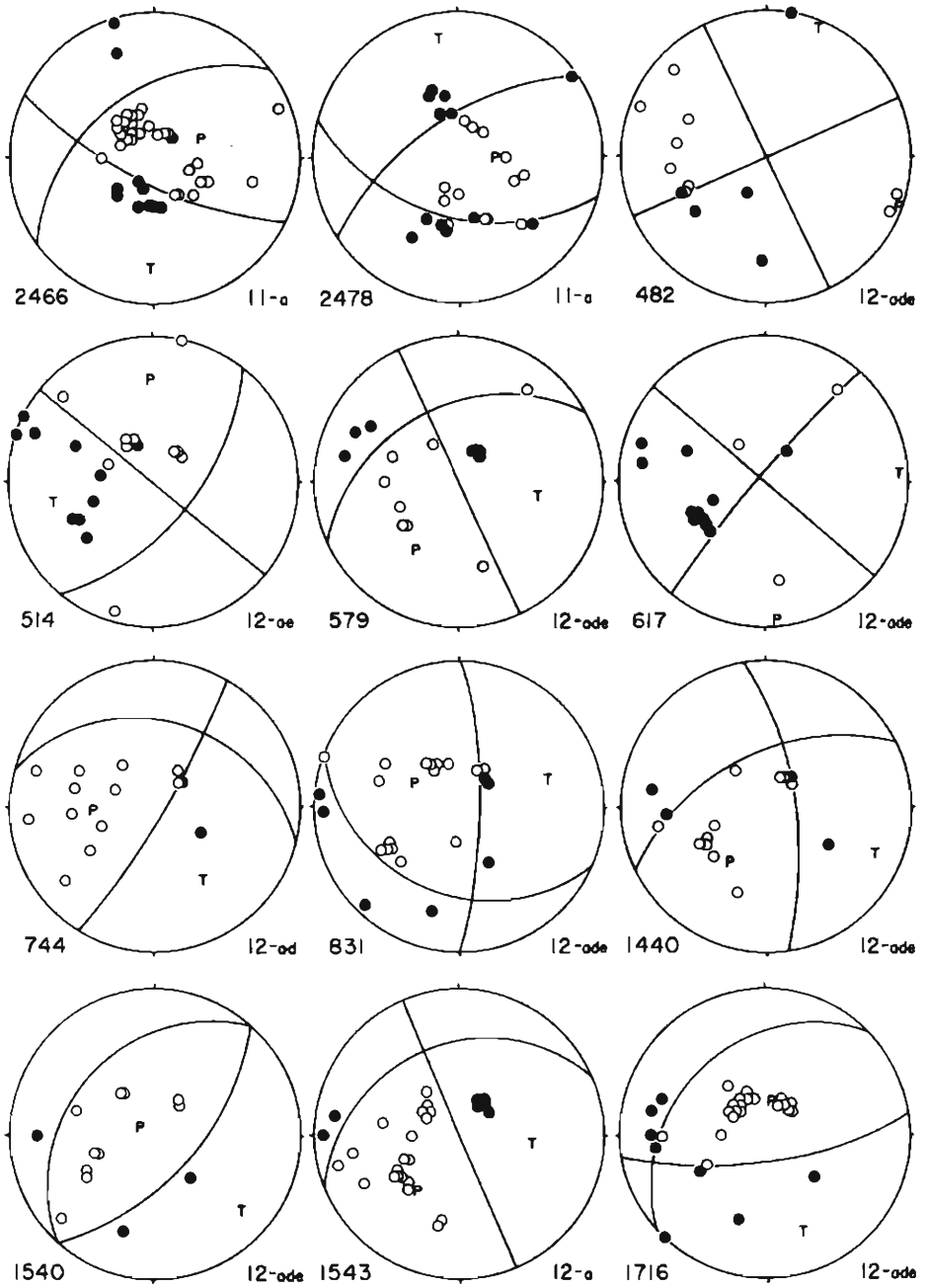
2466 11-a
2478 11-a
482 12-ade
514 12-ae
579 12-ade
617 12-ade
744 12-ad
831 12-ade
1440 12-ade
1540 12-ade
1543 12-a
1716 12-ade

Fig. 37-e.

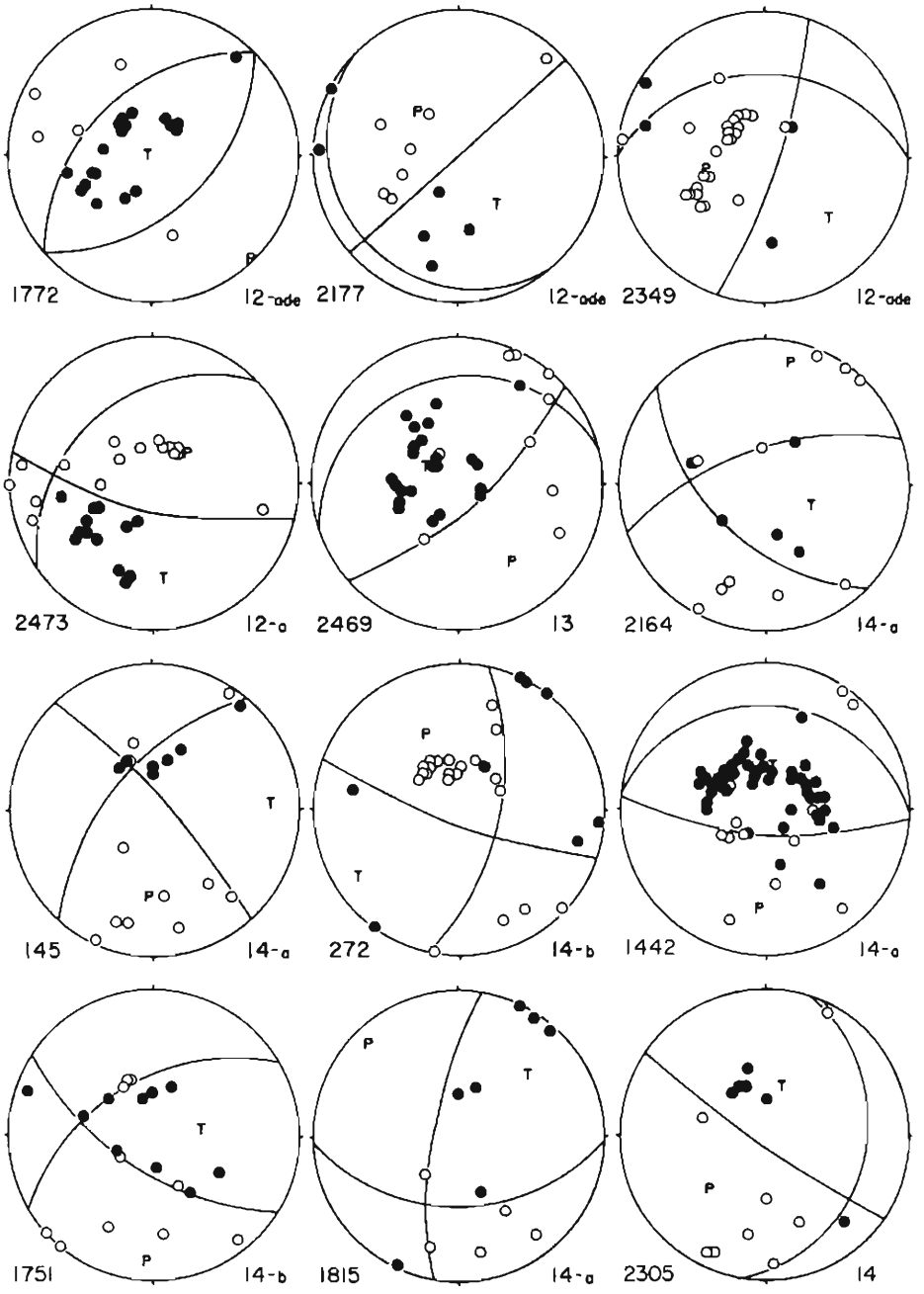
1772
12-ade
2177
12-ade
2349
12-ade
2473
12-a
2469
13
2164
14-a
145
14-a
272
14-b
1442
14-a
1751
14-b
1815
14-a
2305
14
T
P

Fig. 37-f.

19) loc. cit. 5).
20) Soboleva, O. V.: The Stresses in the Foci of the Hindukush Earthquakes of July 6, 1962, and of March 14, 1965, Bull. (izv.) Acad. Sci. USSR, Earth Phys., No. 2, 1967, pp. 94-97.
21) Fitch, T. J.: Earthquake Mechanisms in the Himalayan, Burmese, and Andaman Regions and Continental Tectonics in Central Asia, J. Geophys. Res., Vol. 75, 1970, pp. 2699-2709.
22) Le Pichon, X.: Sea-Floor Spreading and Continental Drift, J. Geophys. Res., Vol. 73, 1968, pp. 3661-3697.
23) Savage, J. C.: The Mechanisms of Deep-Focus Faulting, Tectonophysics, Vol. 8, 1969, pp. 115-127.